TROPICAL CYCLONE STEERING AS A POTENTIAL VORTICITY ADVECTION PROCESS: THE ROLE OF CUMULUS PARAMETERIZATION IN THE DEFINITION OF AN OPTIMAL STEERING COLUMN

By

Brett T. Hoover

A thesis submitted in partial fulfillment of

the requirements for the degree of

Master of Science

(Atmospheric and Oceanic Sciences)

at the

UNIVERSITY OF WISCONSIN – MADISON

2008

Abstract

Tropical cyclone (TC) *steering flow* is defined as that part of TC motion attributable to the advection of TC potential vorticity (PV) by the asymmetric flow in the vicinity of the vortex. The asymmetric flow is calculated by horizontally and vertically averaging the horizontal winds over a three-dimensional domain (referred to as a "*steering column*") centered on the position of the TC vortex. The relationship between the optimal steering column and the PV structure of the TC is diagnosed in a modeled TC, and the evolution of this relationship is related to the evolution of the TC PV structure as the TC matures. Furthermore, the TC track in a numerical weather prediction model is shown to be affected by the choice of cumulus parameterization, due to the dependency of the TC PV structure on the distribution of diabatic heating.

Two model simulations of a TC are performed which differ only in the choice of cumulus parameterization, and the observed track-split between the two simulations is investigated from the perspective of TC steering and propagation mechanisms. The differences in diabatic heating brought on by varying cumulus parameterizations is shown to elicit differences in the PV structure of the model simulation both in the large scale environment and in the storm scale differences in PV within the TC itself. It is shown that large scale differences in the model simulations are initially unimportant and only grow in importance after the track split between the two simulations. The small scale differences in PV structure are responsible for the track split, after which the two simulations continue to diverge as the TCs evolve in differing environments. Despite these differences, a consistent relationship between the structure of the optimal steering column and the TC PV structure appears in both simulations. The simulations pass through three steering "regimes" based on

the evolution of the PV within the TC. In regime 1, the TC is primarily steered at the level of the maximum PV. Regime 2 is a transitional phase when the TC begins to be steered at the PV "center of mass". In regime 3, the optimal steering column depends on the vertical depth of the column, with shallow columns centered at the PV "center of mass" and deep columns centered on the vorticity "center of mass".

Acknowledgements

My first acknowledgement goes to my advisor, Dr. Michael Morgan. Beyond being a great academic advisor (which he is), and being a great teacher committed to the success of his students (which he is), one of Michael's most important contributions to this work is that he never gave up on me, even when I was willing to give up on myself. My first research experience has neither been easy nor fun, but I feel like I've become a better person for having finished it. Michael understood the importance of that.

Secondly, I want to thank my readers, Dr. Jonathan Martin and Dr. Greg Tripoli. Both of you have given me valuable feedback on my work, and have demonstrated such excellence in academia that I hope to continue to learn from you for a long time (would this be a good time to ask you to be on my Ph.D. committee?). Jon, you are able to tackle any subject, no matter how far out of your area of expertise, with the same enthusiasm you apply toward your own research. And Greg is invaluable for giving me a clear (dare I say, brutal?) critique of my work. I find that there is no commodity in this field more valuable than honest criticism, and perhaps my wisest choice in all of this was to ask you to be my readers.

I also want to thank the other students who have worked under Michael. I want to thank Nick Bassill and Ross Lazear for sharing my sense of humor and keeping me laughing through the worst times (maybe someday we can all get jobs writing advertisements for Rocky Rococo's). I also want to thank Dianna Nelson for sharing research woes and being the amazing kind of person who I look forward to seeing every day:

The ocean's rage cannot force you to keel;

Your laugh turns seas to glass and sets the sun…

I want to thank Andy Hulme, who wasn't a student of Michael's, but somehow became like the childhood friend that practically lives at your house and your parents treat like one of their own, despite the fact that he has a perfectly good family just down the street. Nick and Andy are especially acknowledged for helping me prepare for the qualifying exam.

I want to thank my mother, who has worked far too hard and far too long to see this day. And I want to thank my father, who didn't live quite long enough to make it here with us.

This is for you, dad.

List of Figures

Table of Contents

Chapter 1

1.1 Tropical cyclone motion

a) Definition of steering and propagation

The processes governing TC motion can be divided into two categories, “steering” and “propagation”. Flatau et al. (1994) define steering as the process of advection of the TC vortex by the “environmental flow”, where the environmental flow is the asymmetric flow over the TC vortex (i.e. the flow in the vicinity of the TC with the symmetric flow of the vortex removed). Flatau et al. define propagation as processes involving an interaction between the TC and the environment which have an effect on the TC’s track. Thus it is implied that steering is only dependent upon environmental characteristics, while propagation involves characteristics of both the environment and the TC itself. However, there is no objective measure to separate the flow into a “TC vortex” component and an “environmental” component. Clearly, the divisions defined by Flatau et al. (1994) are not absolute and the partitioning of TC motion between steering and propagation is non-unique.

b) Steering

We define *steering* as the process by which the TC vortex is advected by the environmental flow (Chan 2005). For barotropic, non-divergent, *f*-plane conditions, conservation of vorticity dictates that TC motion is governed solely by steering (Flatau et al. 1994). Even in baroclinic flow, this concept of TC steering is important.

To distinguish the environmental flow from that of the embedded TC vortex, an averaging of the horizontal wind field is performed to remove the symmetric vortex flow. The remaining flow defines that of the environment. Since this environmental flow varies in the vertical, an averaging of the horizontal winds must also be performed over some depth of the troposphere (Chan 2005). The horizontal and vertical extent over which the averaging is performed to calculate a steering flow is known as the “steering column”. Because this averaging may be performed over a number of volumes, the definition of the environmental flow is non-unique (Flatau et al. 1994). Moreover, even if the horizontal dimensions of the steering column were perfectly known, it is not always clear what the vertical dimensions should be. These ambiguities have prompted many studies over the last decade to understand the nature of TC steering, and discover the optimal dimensions of the steering column.

The atmosphere is neither barotropic nor non-divergent, and the Coriolis parameter varies. As a consequence, TC steering is not the only process contributing to TC motion. TCs have been shown to move slightly differently from the environmental flow, due to propagation mechanisms (Flatau et al. 1994, Wu and Wang 2000, Chan et al. 2002, Chan 2005). However, the steering process has been shown to be the dominant mechanism for steady TC motion (Chan et al. 2002).

For our purposes, the TC is defined as a cyclonic PV tower, and advection of that tower by asymmetric flow determines the steering of the TC. The TC can interact with the environment to create an asymmetric flow, which by our definitions would be considered a steering mechanism. A few examples follow.

“Beta-drift” is the process by which the TC distorts the background PV gradient, creating PV minima and maxima on either side of the TC. These so-called “beta-gyres” create a ventilation flow over the TC, which causes the TC to propagate poleward relative to the steering flow (Fiornio and Elsberry 1989, Shapiro 1992). This is an example of the TC interacting with the environment to create an asymmetric flow.

Shapiro (1992) and Wu and Emanuel (1993) described a process by which vertical shear over a TC causes the TC vortex to become divorced from its upper-level anticyclone. When viewed as PV anomalies, these anomalies (of opposite sign) create penetration flows which can cause the two to advect each other. For example, westerly vertical shear would cause the upper-level anticyclone to be advected to the east of the lower level vortex. The two would then advect each other poleward through their respective symmetric circulations (Wu and Emanuel 1993).

c) Propagation

Propagation mechanisms include a number of processes governing TC motion not attributed to steering, causing the TC to move relative to the ambient environmental advection of the vortex. The two examples below are processes which contribute to the PV tendency of the TC but are not considered steering mechanisms by the definition given above.

While steering is an advection process, advection can be split into two categories. Advection of the symmetric component of the vortex by the asymmetric component of the flow is the classic description of TC steering described above. However, an asymmetric component of the TC vortex exists as well. This asymmetric component of the vortex could be advected by the symmetric flow of the TC vortex itself, leading to propagation of the vortex as a whole (Chan et al. 2002). This process is called “self-advection”. While this mechanism is an advection process, it is caused by the symmetric component of the flow, not the environmental flow, and therefore is not a steering mechanism.

Wu and Wang (2000) and Chan et al. (2002) describe how asymmetric diabatic heating can play a role in TC motion. Chan et al. (2002) found that the importance of diabatic heating and the self-advection process described above often fluctuate together. Taken together with all of the other processes described, it becomes clear that TC motion is a difficult forecasting problem. Many of these propagation mechanisms aren't easily individually quantifiable, even in a modeling experiment. The importance of TC steering in TC motion, together with the inability of forecasters to calculate the effect of TC steering, makes it an important focus of research for further improving track forecasts and understanding what factors contribute to successful or unsuccessful track forecasts.

d) The steering column

The steering column is used to define the symmetric flow around the TC vortex. The difference between the observed flow and the symmetric flow defines the asymmetric flow over the TC. As discussed previously, the TC moves as a single entity even in the presence of vertical shear of the environmental flow. Thus, it is necessary for the steering column to encapsulate the portion of asymmetric flow most important to TC motion, referred to as the "steering flow". Defining the characteristics of the steering column which provides the steering flow has been a major area of TC research for decades.

Chan and Gray (1982) found that an azimuthal average of the horizontal winds between roughly 550-770 km, and vertically averaged between 500 and 700 hPa, provides the most accurate steering flow. However, studies have since shown that the vertical depth of the steering column varies with the intensity of the TC (Simpson 1971, Dong and Neumann 1986, Pike 1987, Velden and Leslie 1991). Specifically, the steering flow of intense (weak) TCs tends to be described by deeper (shallower) steering columns. Velden and Leslie (1991) proposed a reason for this relationship. They argued that as a TC intensifies, the TC's vortex increases in depth, which they called the "vortex intensity – vortex depth", or VI-VD relationship. As the TC vortex deepens, so does the associated steering column which defines the environmental flow which steers it. As a result, steering columns which vary with depth based on the intensity of the TC tend to minimize forecast track error.

e) Steering and PV advection

The TC vortex can be viewed as a positive PV "tower" above a potential temperature maximum at the top of the boundary layer and beneath an elevated dynamic tropopause (Shapiro and Franklin 1995; Wu and Emanuel 1995a,b; Shapiro 1996; Wu and Kurihara 1996).[1] One can then assume that under quasi-balanced conditions, the motion of the TC is governed by the advection of the TC PV tower. The definition of TC steering from a PV perspective is supported by evidence that the VI-VD relationship has been observed in the distribution of PV associated with Hurricane Bob (Wu and Kurihara 1996).

TC steering has been diagnosed with the PV tendency equation (Wu and Wang 2000, Chan et al. 2002):

$$\frac{\partial q}{\partial t} = -\mathbf{V} \cdot \nabla q + \frac{Dq}{Dt},$$

where **V** denotes the horizontal wind and q the PV. From this perspective the TC moves to the region of maximum wavenumber-1 PV tendency, which is changed primarily through

[1] From the perspective of moist, saturated PV, the dynamics of the TC are governed by the distribution of saturated equivalent PV at the top of the boundary layer.

two processes: horizontal advection of the TC PV by environmental flow, and diabatic redistribution of PV in the vertical (Wu and Wang 2000, Chan et al. 2002). Furthermore, horizontal advection can be broken into asymmetric advection of the symmetric component of PV, which is the steering process (Shapiro 1992, Chan et al. 2002), and symmetric advection of the asymmetric PV, which is a self-advection process. The PV tendency equation partitioned in this manner may be written as:

$$\frac{\partial q}{\partial t} = -\mathbf{V}_s \cdot \nabla q_s - \mathbf{V}_s \cdot \nabla q_{as} - \mathbf{V}_{as} \cdot \nabla q_s - \mathbf{V}_{as} \cdot \nabla q_{as} + \frac{Dq}{Dt} = -\mathbf{V}_s \cdot \nabla q_{as} - \mathbf{V}_{as} \cdot \nabla q_s - \mathbf{V}_{as} \cdot \nabla q_{as} + \frac{Dq}{Dt},$$

where subscripts *s* and *as* denote respectively, the symmetric and asymmetric parts of the horizontal wind and PV. The loss of the term describing the symmetric flow field advecting the symmetric PV occurs because we assume that the symmetric part of the flow does not advect the symmetric PV. Chan et al. 2002 found that the steering process, $-\mathbf{V}_{as} \cdot \nabla q$, dominates for steady TC motion, while in erratic TC motion, the two propagation mechanisms as well as the diabatic generation term, can play a large role. TC steering, during steady TC motion, can be called “PV-steering”.

It is hypothesized that choice of cumulus parameterization can have a significant impact on PV-steering in a modeled TC. This is because the cumulus parameterization can affect the PV structure of the TC through dictating the distribution of latent heat, which will redistribute PV in the vertical. This can affect the level at which the horizontal advection of the TC PV by the environmental flow is strongest – or the steering level (Chan 2005). Varying the cumulus parameterization has been shown to have an impact on TC motion (Prater and Evans 2002, Chan 2005), but no study of the relationship between TC PV structure and steering column structure has been attempted.

One hypothesis is that PV may be used as a weighting function for weighting the impact of the environmental flow at each level on the steering of the TC as a whole. Ueno (2003) tried a similar tactic whereby the sea-level pressure tendency equation was used to create a weighting function for such a "weighted steering flow". In that study, it was found that choice of cumulus parameterization had an impact on TC track, and that the weighting function changed between different cumulus parameterizations. A similar experiment will be performed here, except that rather than using the sea-level pressure tendency equation, the modeled TC's PV will be directly used as a weighting function.

Next we will take an in-depth look into the role of cumulus parameterization schemes (CPSs) in numerical models, with special attention paid to the two CPSs used in this study.

1.2 Cumulus parameterization schemes

a) Definition and role of cumulus parameterization schemes in numerical models

Cumulus convection presents a problem in numerical weather prediction (NWP) models when it cannot be explicitly resolved. Atmospheric convection is associated with a number of important processes including momentum, moisture, and heat transport, which must be accounted for accurately in an NWP model forecast for that forecast to faithfully mimic the observed atmospheric evolution. These processes; however, occur on space and time scales not resolvable by the spatial and temporal discretizations upon which NWP model variables are calculated. As a consequence, these processes must be *parameterized* – using grid-resolvable variables to diagnose the occurrence of sub-grid scale processes and subsequent impact of these processes at the grid scale. A cumulus parameterization scheme, (CPS), designed to parameterize the role of cumulus convection in NWP models, represents an important class of parameterization schemes used in NWP models for grid spacings greater than 4km.

CPSs can be especially important in the numerical modeling of tropical cyclones (TCs). Latent heat release in cumulus convection is the primary process by which a TC intensifies through production of buoyancy above the boundary layer (Smith 2000). This latent heat release also plays a role in shaping the TC's vortex by eroding potential vorticity (PV) above the level of maximum latent heat release and redistributing it below. In addition, CPSs contribute to simulating processes in the planetary boundary layer of a TC (Smith 2000). The inclusion of parameterized downdrafts has been shown to have a significant impact on the distribution of pressure, precipitation, and surface features in NWP model forecasts and simulations (Grell 1993; Wang and Seaman 1997). These downdrafts may even influence the track of a modeled TC through advection of saturated equivalent potential temperature in the boundary layer (Emanuel, personal communication). The choice of a CPS in a NWP model can therefore have a significant impact on the structure, development, and maintenance of modeled TCs.

b) Types of cumulus parameterization schemes used in study

Following is a brief description of the two CPSs used in this study.

1) THE BETTS-MILLER CUMULUS PARAMETERIZATION SCHEME

The Betts-Miller (BM) CPS is a lagged convective adjustment scheme that allows both shallow and deep sub-grid scale cumulus convection to influence relevant model variables at grid scale by adjusting thermal and moisture fields toward reference profiles separately defined for shallow and deep convection. Observations of atmospheric profiles during deep convection events define the parameters of the Betts-Miller CPS. Shallow convection makes use of reference profiles constructed from a mixing line subject to an energy constraint, while reference profiles for deep convection are partially derived from observational studies and partially internally determined (Smith 2000, Betts and Miller 1984a).

The BM CPS seeks to maintain "realistic" temperature and moisture profiles in the presence of convection (Betts and Miller 1984a). The scheme develops these profiles by way of a first guess profile defining the freezing level as the level of minimum virtual potential temperature, and increasing linearly back to environmental potential temperature at cloud top. Weighting coefficients are derived from observational data to provide the most realistic results (Betts and Miller 1984a).

The strength of the BM CPS, according to Emanuel (1994), is that BM is able to produce convection in regions of instability to drive the atmosphere back to neutrality, without artificial constraints (such as) on convection (Smith 2000). However, the model requires a reference profile to which the atmosphere is driven, and there is no such thing as a universal reference profile for relative humidity (Smith 2000). In addition, the scheme does not parameterize convective downdrafts (Wang and Seaman 1997), which may have significant effects on the boundary layer moisture and temperature distribution. This scheme has been shown to be able to rapidly intensify a TC from a weak vortex (Baik et al. 1990a).

2) THE GRELL CUMULUS PARAMETERIZATION SCHEME

In contrast to the BM lagged convective adjustment scheme, the Grell scheme is a *quasi-equilibrium* scheme, employing the quasi-equilibrium assumption of Arakawa and Schubert (1974) to provide closure: the role of cumulus clouds in this scheme is to remove conditional instability from the large-scale flow at the rate which that conditional instability is introduced (Smith 2000). Unlike the BM scheme, the Grell parameterization includes the effects of parameterized downdrafts (Wang and Seaman 1997; Grell 1993). Wada (1979) has shown that such quasi-equilibrium closure schemes can be used to realistically simulate TCs (Smith 2000).

Unlike the Betts-Miller parameterization, the Grell parameterization calculates environmental thermodynamic profiles from model variables. Quasi-equilibrium schemes, like the Grell or Arakawa-Schubert scheme, seek to consume moist-static energy at the rate which it is produced by the environment through convective clouds which operate on time scales much shorter than that of the overall environment (Smith 2000). The scheme calculates individual cloud top heights and available buoyant energy, and recalculates thermodynamic profiles and available buoyant energy after convection (Haagenson et al. 1994).

Because the BM and Grell CPS use different methodologies for providing closure to the model and handle downdrafts differently, it is hypothesized that they will provide a useful example of how CPSs can influence the track and intensity of a modeled TC both through how the CPSs handle tropospheric-deep convection and through differences in the handling of the TC's planetary boundary layer.

c) Behavior of cumulus parameterization schemes in model

The Penn State/NCAR MM5 model used in this studied has a 30km grid with 20 evenly spaced sigma levels. It employs simple ice physics and the MRF boundary layer scheme, with cloud model radiation and a multi-layer soil temperature model. The model is initialized with NCEP 1.0^{o} x 1.0^{o} final analysis data at 0000 UTC 14 September 2006, simulating the cyclogenesis of Hurricane Helene (2006) starting from tropical depression status and is run for 96 hours. A synoptic overview of the case considered is provided in chapter 2. No bogus vortex was introduced into the model. Here, we will focus on the storm-scale differences in precipitation and TC boundary layers which appear as a result of varying the CPS of the NWP model simulation.

Significant differences in precipitation appear in the first 48 hours of the model simulation. Figure 1.1 is a two-panel plot showing the model domain integrated total precipitation for each simulation each hour for the first 48 hours. Clearly, the BM scheme produces far more precipitation than the Grell scheme for this case. While the BM scheme appears to continue to create more precipitation, the two simulations begin to produce about the same amount by 30 hours into the simulation. Figure 1.1b shows the ratio of parameterized convective precipitation to the total precipitation (sum of parameterized and explicitly resolved precipitation at grid scale). Here further differences between the two simulations become apparent. While the fraction of convective precipitation falling in the Grell simulation drops off from 100% to 65% by 34 hours into the simulation, the BM simulation never drops below about 93% convective precipitation. Comparing the plots from both panels, it appears that the Grell parameterization produces more precipitation when the ratio of convective to total precipitation drops. The maximum precipitation rate at 10 hours is coincident with a drop in convective precipitation, as is the secondary maximum in precipitation rate between 30 and 40 hours. The BM simulation does not appear to have this behavior.

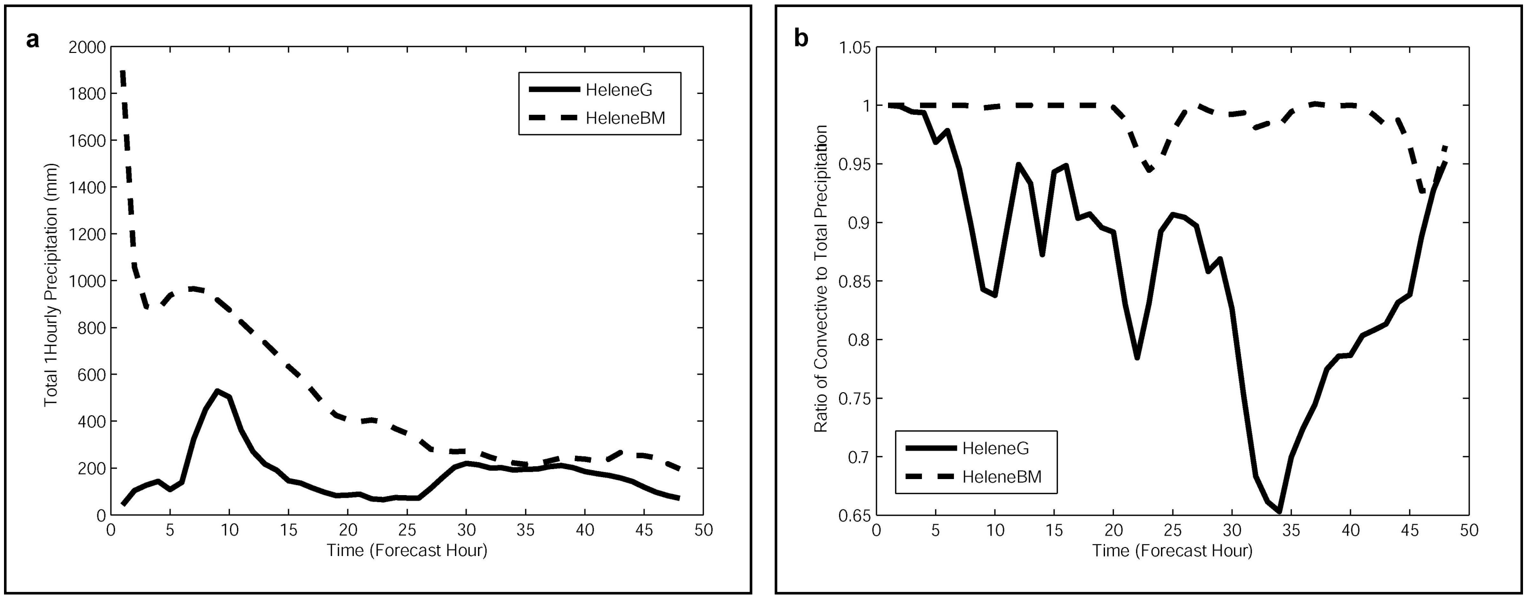

Figure 1.1. Two panels describing the precipitation in both model runs. Panel (a) shows the total precipitation falling each hour over the entire model domain (mm) for the first 48 hours, while panel (b) shows the ratio of convective to total precipitation over the same time period.

The ratios of convective and explicit precipitation to the total precipitation in each simulation agrees loosely with Wang and Seaman (1997), who provide a detailed comparison study of the two CPSs for a simulated mesoscale convective system (MCS). In that study, they showed a steep drop-off in convective precipitation after only a few hours with the Grell CPS, with significantly higher convective precipitation ratios when using the BM parameterization (see their Fig. 10; Wang and Seaman 1997). While this so-called "rain-ratio" is higher in our study than in the MCS study, this may be due to the obvious differences between the case of a mid-latitude MCS over land and a TC, or possibly to differences in parameters set within the CPSs. The Grell parameterization is especially sensitive to the precipitation efficiency parameter, the adjustment of which can significantly change the rain-ratio (Wang and Seaman 1997).

The boundary layers of both simulations differ quite significantly. Figure 1.2 shows the evolution of the surface saturated equivalent potential temperature (θ_e^*) in both models. Large differences in this field can be attributed at least partially to how the two CPSs handle downdrafts. The Grell scheme parameterizes convective downdrafts, which are manifest as regions of low surface θ_e^* which appear near the cyclone center and spiral out. The BM scheme has no such downdrafts, and no low θ_e^* regions appear in the TC.

Notable differences develop between the two simulations with regard to the θ_e^* maxima. In the Grell simulation, significantly lower θ_e^* prevails in the TC's boundary layer, in a large part due to the effect of parameterized downdrafts. The pressure minimum appears coincidently with the θ_e^* maximum, and they continue to be coincident throughout the entire simulation. In the BM simulation, on the other hand, θ_e^* is significantly higher in the

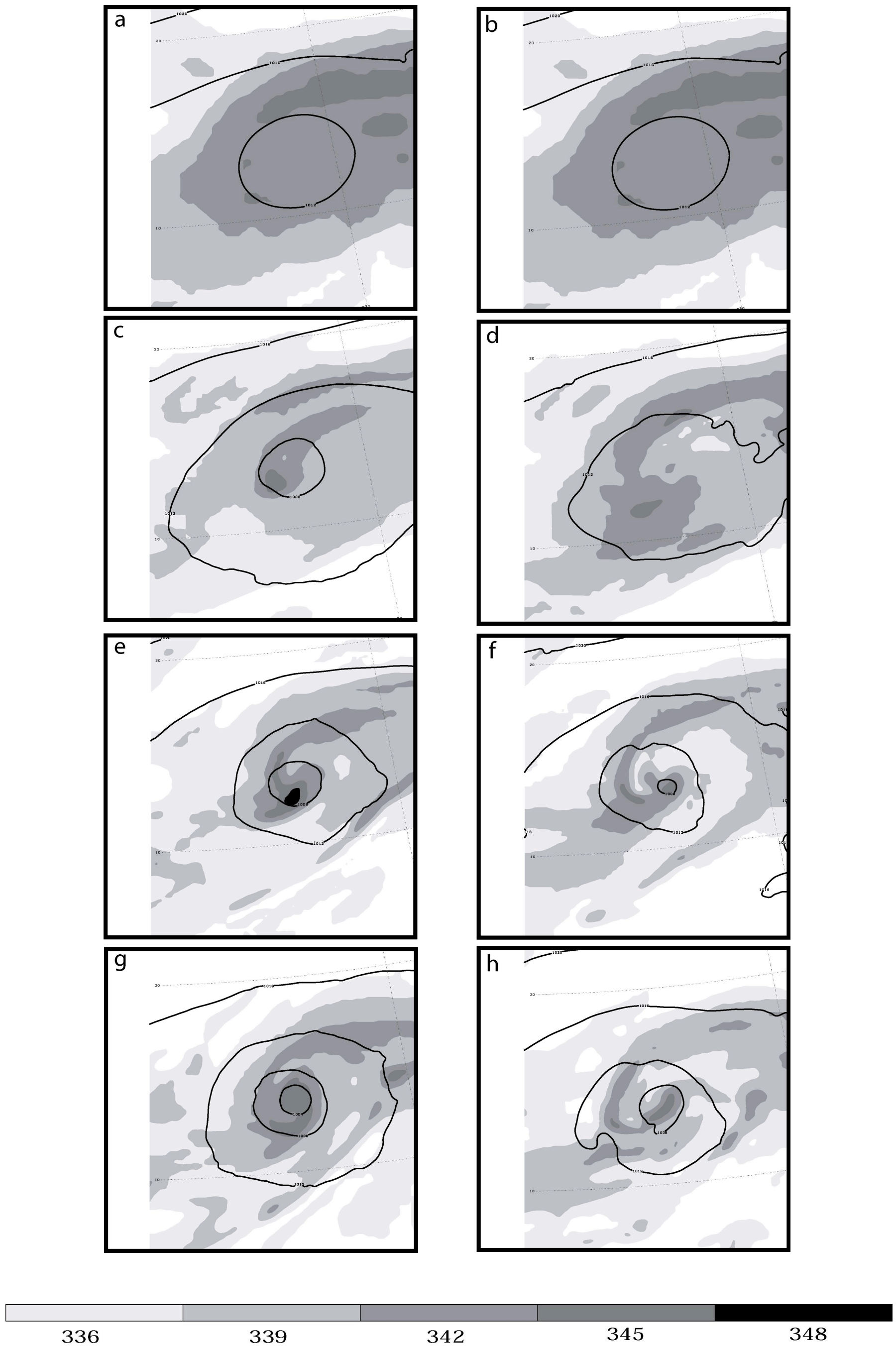

Figure 1.2. Surface saturated equivalent potential temperature and sea level pressure fore Helene-BM (left panels) and Helene-G (right panels) for 00 hours (panels a and b), 06 hours (panels c and d), 12 hours (panels e and f) and 18 hours (panels g and h) into the simulation. Temperature is shaded every 3 K and sea level pressure is contoured every 4 hPa.

boundary layer, and the θ_e^* maximum appears almost immediately in the northwest quadrant of the TC. This θ_e^* maximum appears to be intensified as it is advected into the center of the TC. By about 24 hours into the simulation, the θ_e^* maximum is coincident with the pressure minimum, and the two remain coincident from then on.

This difference in boundary layer θ_e^* may have important implications for TC steering around the time when the θ_e^* maximum of the BM simulation exists outside of the pressure minimum, and is advected by strong winds near the TC center. In addition, the effect of parameterized downdrafts in the Helene-G simulation is manifest as a region of low θ_e^* (dry) air appears in the northeast quadrant of the cyclone center, a feature which is completely missing from the Helene-BM simulation. This dry air appears to then wrap around the cyclone, and may be partially responsible for the slower intensification of the Helene-G simulation. The lower surface θ_e^* suppresses cumulus convection, by reducing the production of positive buoyancy and consequently inhibiting deepening.

The remainder of this thesis is divided into two chapters. Chapter 2 is intended to be a stand alone paper to be submitted for publication in a refereed journal, while Chapter 3 summarizes the results and offers a discussion of potential future work. In Chapter 2, we introduce the “steering plot” as a useful tool for diagnosing the characteristics of the optimal steering column, and relate those characteristics and their evolution to the evolution of the TC PV structure. A theory is then proposed to explain this relationship. The track split observed between the two TC simulations is analyzed with respect to PV steering and propagation mechanisms which arise from varying the CPS in the model.

Chapter 2.

2.1 Introduction

Tropical cyclone (TC) motion is a combination of two mechanisms: "steering" and "propagation" (e.g., Flatau et al. 1994). "Steering" describes the process by which the environmental (i.e., non-TC) flow advects the TC vortex. A *steering flow* is often defined as the mean asymmetrical flow centered on the location of the TC. Owing to the dearth of *in situ* observations over tropical oceans, and to the lack of a definitive method by which the TC winds can be separated from the observed flow, the steering flow is not only difficult to identify, but also non-unique. "Propagation," the component of TC motion that deviates from the steering flow, involves a number of processes including those for which the asymmetrical hurricane flow interacts with the hurricane itself and asymmetrical diabatic heating (to be described later in this section).

Several studies have been performed to identify a TC's so-called *steering column* - an optimal horizontal and vertical volume over which to perform the averaging of the horizontal wind field to calculate a steering flow best approximating the observed motion of a TC. Chan and Gray (1982) have shown that the horizontal wind, averaged between a depth of 500 and 700 hPa and a horizontally between 550 and 770 km from the storm center most closely correlates with TC motion. Other studies have shown a more complex relationship between a TC and the winds that drive its movement. For example, Simpson (1971), Dong and Neumann (1986), Pike (1987), and Velden and Leslie (1991; hereafter VL) have noted that relatively weak TCs move with a shallow lower-tropospheric flow, while more intense TCs move with a deeper-layer flow. VL suggest a hypothesis for this relationship: increases in the intensity of a TC are "associated with greater vertical development of the cyclonic vortex, which in turn is advected by an environmental flow of greater depth." Using a barotropic track-forecasting model, VL demonstrated that mean forecast errors in TC tracks may be reduced if the depth of the vertically-averaged initial wind analysis is based on the TC intensity. A goal of this study is to relate TC steering to the TC's potential vorticity (PV) (vertical) structure

The structure of a TC may be described succinctly by its PV, while the details of TC steering may be related to its PV tendency (Wu and Wang, 2000 and 2001 and Chan et al. 2002). In this study, the PV used is Ertel PV (q) defined as: $q = \frac{1}{\rho}\vec{\omega} \cdot \nabla\theta$, where ρ is the density, $\boldsymbol{\omega}$ is the absolute vorticity vector, and θ represents the potential temperature. The Lagrangian tendency of PV is given by:

$$\frac{Dq}{Dt} = \frac{1}{\rho}\vec{\omega} \cdot \nabla\dot{\theta} + \frac{1}{\rho}\vec{\omega} \cdot (\nabla \times \mathbf{F}),$$

where $\dot{\theta}$ represents the diabatic heating rate and $\mathbf{F}$ represents a frictional force. Observational and modeling studies have shown that the PV structure of a TC is relatively simple; it may be viewed as a cyclonic PV column that is located above a surface equivalent potential-temperature maximum and beneath an elevated dynamical tropopause (Shapiro and Franklin 1995; Wu and Emanuel 1995a,b; Shapiro 1996; Wu and Kurihara 1996). This structure is dependent most on the distribution of heating associated with phase changes of water substance, and friction in the boundary layer. The diabatic heating associated with phase changes in water substance results in a redistribution of PV wherein PV is depleted aloft and increased in the column near the TC's center. Wu and Emanuel (1993) describe the *steady state* PV in a mature TC as a steady cyclonic PV tower maintained by frictional dissipation at the surface and redistribution of PV from aloft by diabatic heating, and by extension, a growing anticyclone aloft.

Wu and Wang (2000) showed that the motion of a TC attributable to environmental steering is well-described by horizontal PV advection. Using PV tendency to diagnose TC motion, Wu and Wang (2000) demonstrated that even though the environmental steering is vertically sheared, a TC moves as a single entity. Chan et al. (2002) partitioned PV tendency into contributions from environmental steering and contributions from diabatic heating, and showed that the horizontal advection of PV dominates in steady TC motion. A similar result was obtained by Wu and Wang (2001), who ran a series of experiments to isolate the non-advective contributions to TC motion. They found that asymmetrical diabatic heating can play an important role in shaping the wavenumber-one component of the PV tendency, which was used to diagnose motion nearly identical to the mean TC speed. However, a steering level could be found at the level where the influence of the asymmetric diabatic heating vanishes, and the TC moves with the steering flow.

Numerical simulations of Hurricane Bob (Wu and Kurihara, 1996) support the existence of a relationship between vortex intensity and vortex depth (VI-VD). In particular, Wu and Kurihara (1996) showed that the height of the PV column associated with Bob decreased as the storm weakened. Chan et al. (2002) suggested that different cumulus parameterization schemes in numerical experiments could lead to different distributions of PV, due to the distributions of the parameterized convective heating.

A track-split between two TC simulations which differed only in choice of cumulus parameterization scheme was observed by Prater and Evans (2002). In that study, a numerical simulation of the intensification and subsequent extratropical transition of Hurricane Irene (1999), it was found that the choice of cumulus parameterization scheme had a profound impact on Irene's track: with the simulation using the Betts-Miller (BM) parameterization having recurved into cool waters too soon to effectively re-intensify as an extratropical cyclone, while a simulation using identical initial conditions but using the Kain-Fritsch (KF) parameterization recurved much later and underwent stronger re-intensification as an extratropical system. The reason for the track-split, Prater and Evans argue, is that the different cumulus parameterizations provide different vertical profiles of heating, which caused the intensity of the two simulations to differ. Prater and Evans point to the necessity of further research to understand the dynamic linkages between differences in parameterized convective heating and subsequent differences in the distribution of PV and the concomitant distribution of wind and thermal structures.

While Prater and Evans (2002) observe a relationship between cumulus parameterization and TC steering, they argue that the major impact of differing cumulus parameterizations is a change in cyclone intensity. They then, like Velden and Leslie (1991), assume the difference in TC intensity translates to a difference in the depth of the TC's cyclonic vortex, and the depth of the environmental steering which advects that vortex.

This study attempts to define a relationship between a TC's PV (and vorticity) structure and its steering by considering the problem of TC steering as a PV (and vorticity) advection process by focusing primarily on the effect of varying cumulus parameterizations on the PV (and vorticity) structure of a modeled TC and how that structure relates to the steering of the cyclone. The VI-VD relationship described by Velden and Leslie (1991) and Wu and Kurihara (1996) is investigated from a PV perspective and is expanded upon to not only include the depth of the PV tower, but the structure of the PV throughout that depth.

In this study, it is hypothesized that TC motion (in a modeled TC) is primarily governed by horizontal advection of the TC's cyclonic PV column. This assumes that the TC PV is in a quasi-steady state, which allows for TC motion to be diagnosed by the advection of a nearly conserved cyclonic PV tower. A number of studies suggest the idea of PV as being nearly conserved in a TC. Shapiro (1992) argued that PV advection in the middle layer of his three layer model was one of the primary causes of TC motion. A track split is observed between two simulations of the same TC using identical initial conditions and varying only in choice of cumulus parameterizations. This difference in model physics is associated with a change in TC motion, and ultimately results in a significant divergence of forecasted track, by changing the vertical level at which the environmental flow steers the TC and moving the two simulations into differing environments once the initial track-split has been achieved.

In section 2, a brief synoptic overview is presented followed by a description of the model set-up and data used in initializing the model. A comparison of the model simulations concludes section 2. The methodology used in evaluating the steering column is given in section 3. An analysis of the steering flows is presented in section 4. Discussion of the results and conclusions follow in section 5.

2.2 Case description, model setup and initial data

a. Synoptic overview

The case chosen for this study was Hurricane Helene (2006), a long-lived Cape Verde hurricane that remained at sea and attained category 3 intensity on the Saffir-Simpson scale on 0600 UTC 18 September 2006. Our analysis focuses on the period 1200 UTC 14 September 2006 when Helene acquired tropical storm status about 680 km west-southwest of the Cape Verde Islands and ends 96 hours later. At 1200 UTC 14 September Helene was situated south of an expansive surface ridge (Fig. 2.1a) and upper-tropospheric anticyclone characterized by low PV in the 348-to-351K isentropic layer. Also of note, was a meridionally elongated upper trough located along 42.5^{o}W in the upper-troposphere near 200 hPa (Fig. 2.1b). This feature perhaps influenced Helene's track by providing strong environmental advection of the TC vortex, and could have influenced the intensity of Helene by producing shear over the TC and stifling intensification (Fig. 2.2). Twelve hours later, the trough was located along 37.5^{o}W, just to east of the longitude of Helene (Figs 2.1 c and d), as Helene neared the eastern edge of the upper tropospheric ridge. The deep-layer (850-300 hPa) shear over Helene was weak, placing Helene in a favorable environment for strengthening (Fig. 2.2b). Over the next 36 hours, while moving west-northwestward over the tropical Atlantic Ocean, Helene steadily intensified and became a hurricane at 1200 UTC 16 September, located about 1600 km east of the northern Leeward Islands. Over that same time interval, the trough continued eastward. By 0000 UTC 16 September a secondary upper trough, which was located at 60^{o}N 35^{o}W on 14/00 had propagated to 35^{o}W, 25^{o}N and was now located just upstream of the primary trough. These two troughs subsequently merged by 0000 UTC 17 September. (Fig. 2.1h) During 17 September, Helene turned northwestward and slowed down. This northwestward motion may be attributed, in part, to rising heights to the northeast of Helene in the wake of the recently merged troughs. Helene continued to

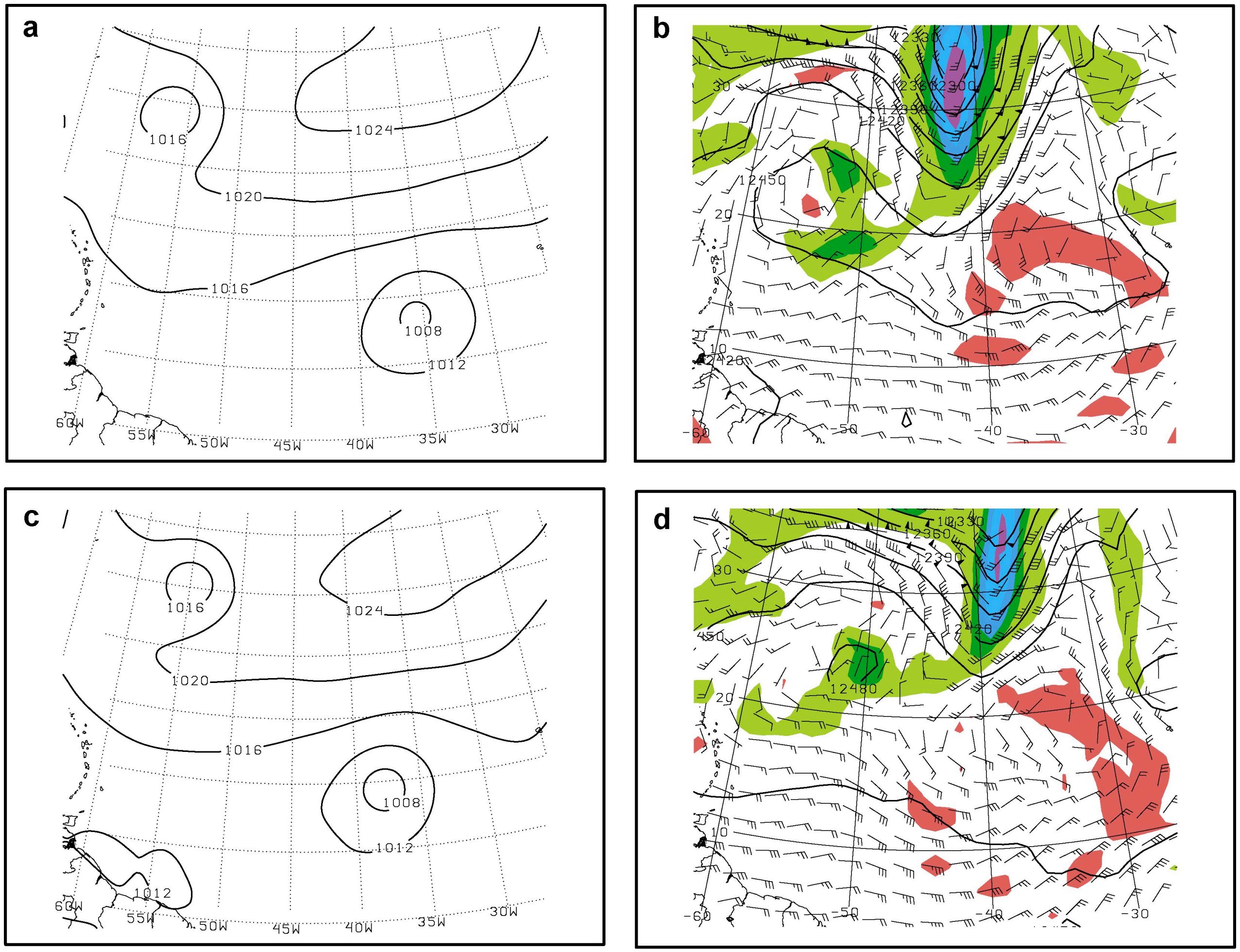

Figure 2.1. Final analysis data synoptic overview – MSLP and upper tropospheric PV. PV is isentropic in 351-354 K layer. Geopotential height (200 hPa) contoured every 30 m. Winds ms^{-1}. MSLP every 2 hPa. Panels a and b correspond to 12 UTC 14 September 2008. Panels c and d correspond to 00 UTC 15 September 2008.

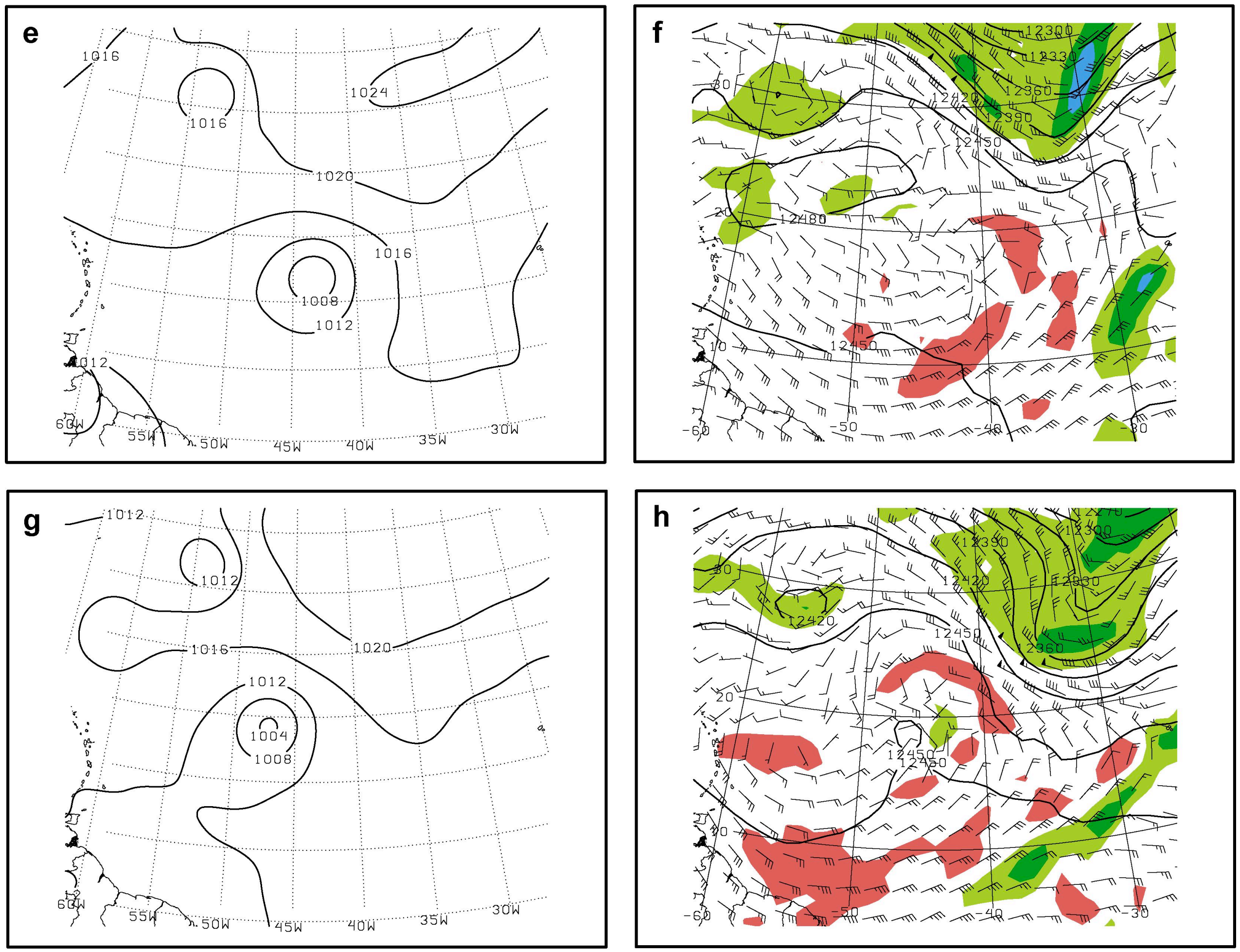

Figure 2.1 continued. Panels e and f correspond to 00 UTC 16 September 2008. Panels g and h correspond to 00 UTC 17 September 2008.

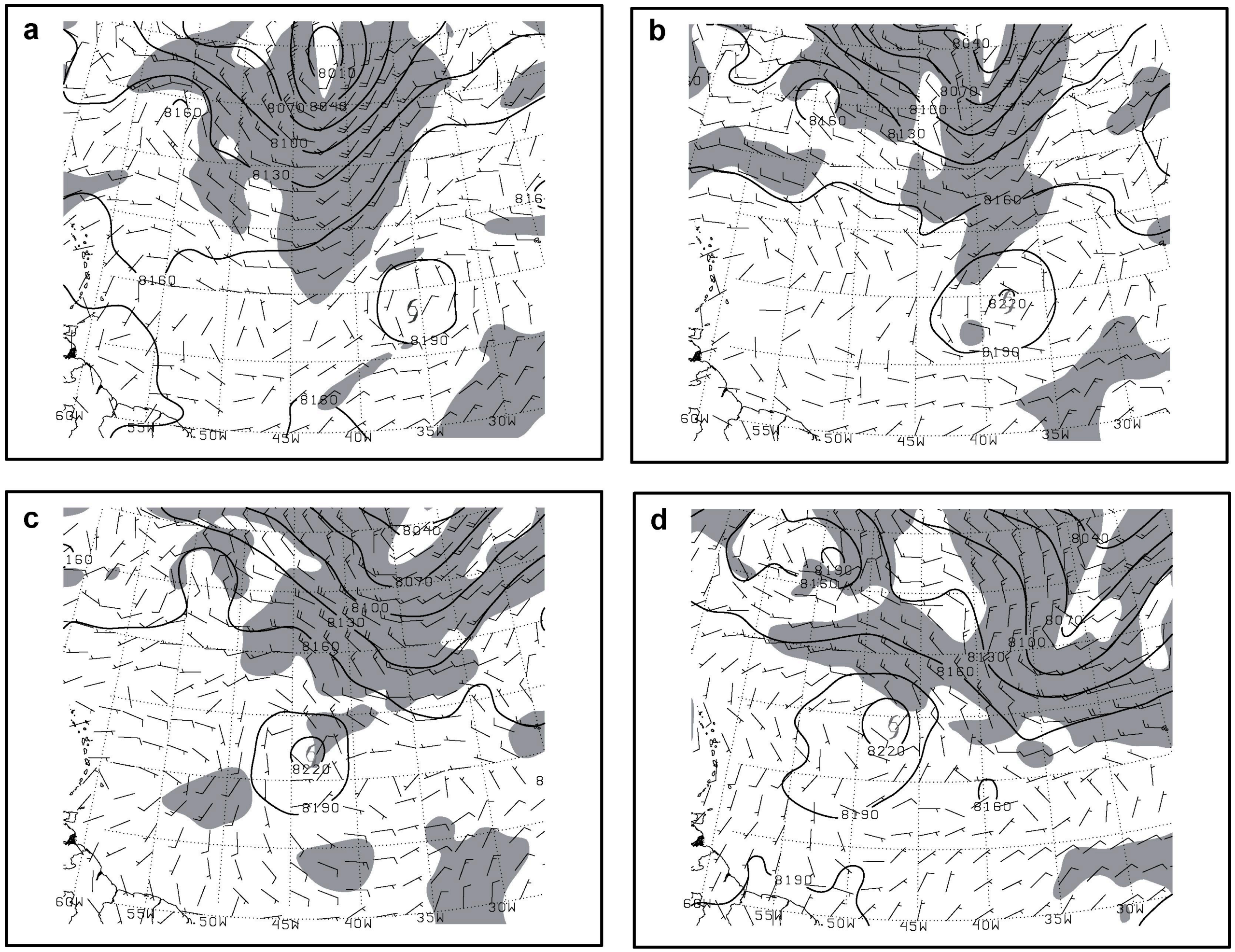

Figure 2.2. Final analysis data synoptic overview - 850-300 hPa thickness contoured every 30m and shear vectors in ms^{-1}. Isotachs of shear vectors shaded. Panel a corresponds to 12 UTC 14 September 2008. Panel b corresponds to 00 UTC 15 September 2008. Panel c corresponds to 00 UTC 16 September 2008. Panel d corresponds to 00 UTC 17 September 2008.

strengthen, attaining category 3 status at 0000 UTC 18 September, and six hours later it reached its peak intensity of 105 kt. The strengthening occurred in an environment of weak, deep tropospheric shear and was associated with increasing 850-300 hPa thickness (Figs. 2.2c and d). The track of Helene from 0000 UTC 14 September through 0000 UTC 18 September is shown in Fig. 2.3.

b. Model setup

The fifth-generation Pennsylvania State University-National Center for Atmospheric Research (PSU-NCAR) Mesoscale Model, version 3 (MM5v3; Grell et al. 1995) is used to perform 30 km, 20 sigma level, 96-hour simulations of Hurricane Helene (2006) starting from the time that the storm was declared a tropical storm (0000 UTC 14 September 2006). The model was initialized using 1^{o} x 1^{o} NCEP final analyses available from the National Center for Atmospheric Research (NCAR) as data set DS083.2. The two model simulations differed only in choice of cumulus parameterization: Betts-Miller (BM) and the Grell (G) parameterizations were chosen to represent a significant track-split between the BM simulation and simulations that used other parameterization schemes. Table 1 shows the model physics packages that were common to each simulation.

Grid spacing	30 km
Number of vertical (sigma) levels	20 evenly spaced levels
Ice microphysics	simple ice
Boundary layer	MRF scheme
Radiation	cloud model

Soil model	multi-layer temperature model
Initialized data	NCEP final analyses at $1^{o} \times 1^{o}$
Initialization time	0000 UTC 14 September 2006
Length of simulation	96 Hours
Bogus vortex	None

Since the goal of this study is to find a relationship between a modeled TC's PV structure and its optimal steering column, an accurate representation of Helene (2006) is not an objective, and as a consequence, the resemblance of the modeled TC to the observed intensity, track, and evolution of Helene (2006) is irrelevant. Since the modeled TC used in this experiment is born from the initial conditions containing the nascent Helene (2006), the modeled TC will be hereafter referred to as 'Helene', even though the model simulation may differ considerably from actual observations of Helene's track and intensity.

c. Synoptic overview of simulations

1) TRACK AND CENTRAL MEAN-SEA LEVEL PRESSURE

Figure 2.3 shows the track of the minimum mean sea level pressure (MSLP) for the two simulations of Helene every six hours between 0000 UTC 14 September 2006 to 0000 UTC 18 September 2006, 96 hours from initialization. The purple track represents the BM simulation of Helene (hereafter, Helene-BM), while the green track represents the Grell simulation (Helene-G). Both simulations appear to follow one another very closely for the first 12 hours. However, by 18 hours into the simulation a significant track-split occurs. Helene-G moves to the northwest at roughly twice the speed of the Helene-BM simulation.

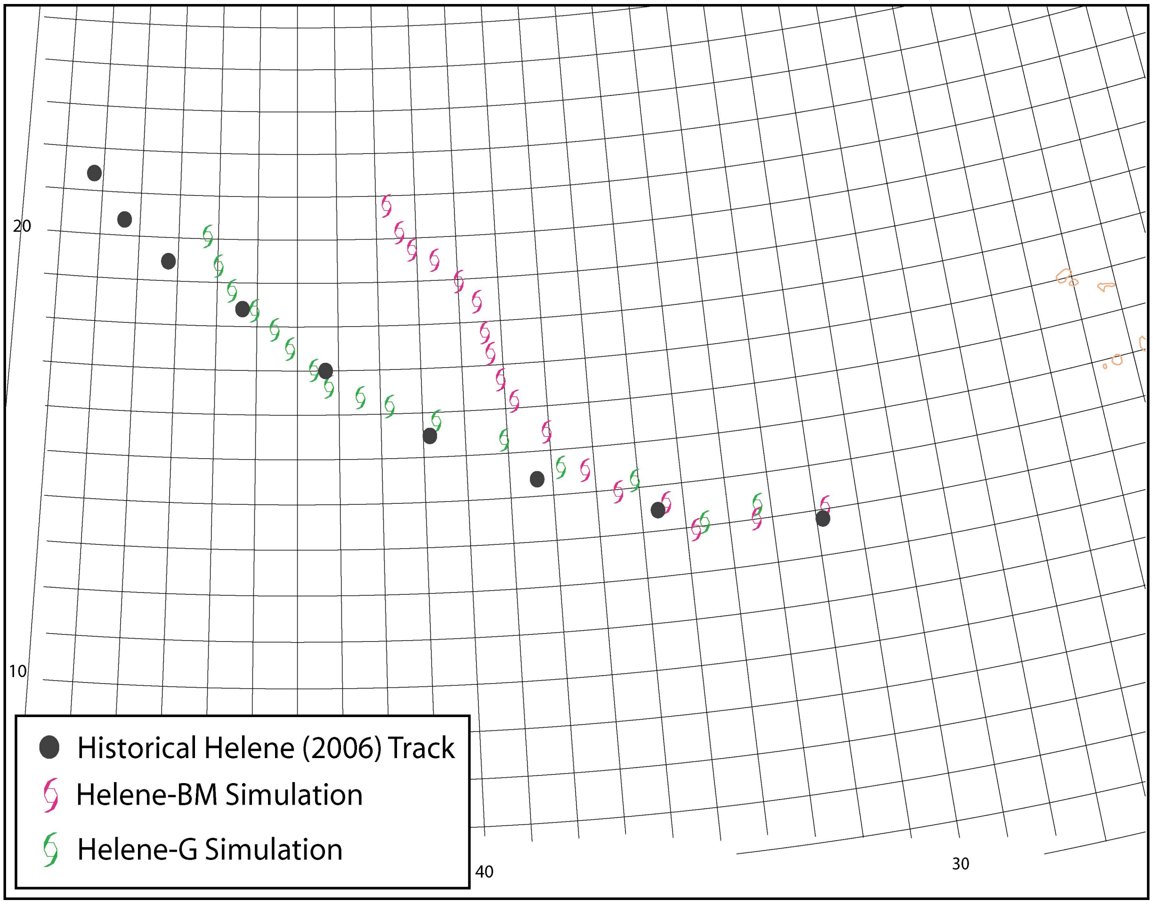

Figure 2.3. Track of Helene (2006) and MM5 simulations of Helene (2006) between 12 UTC 14 September 2006 and 12 UTC 18 September 2006. The black dots indicate the observed location of Helene every 12 hours. The green symbols represent the location of Helene-G every six hours, and the purple symbols represent the location of Helene-BM every six hours.

From that point onward, the tracks of the two simulations continue to diverge as the Helene-BM simulation slows its westward progression and slowly moves to the north, while the Helene-G simulation continues its northwestward progression at a faster speed. By 96 hours into the simulations, the simulated TCs are at nearly the same latitude, but separated by 4.5 degrees of longitude or about 475 km. While not relevant for the study to follow, we note that in terms of track, the Helene-G simulation most closely matched the analysis.

Figure 2.4 shows a time series of the mean sea-level pressure for the simulations Helene-G and Helene-BM. Helene-BM intensifies more rapidly than Helene-G for the first 66 hours of the two simulations. The BM simulation reaching an absolute minimum sea-level pressure of 982 hPa at 78 hrs, while the Grell simulation only reaches an absolute minimum sea-level pressure of 988 hPa by the end of the simulation. Both simulations have comparable intensities at 96 hrs as Helene-BM begins to fill.

A brief synoptic overview of the two simulations as well as a description of each simulations' TC cyclonic PV structure follows. The purpose of this overview is to highlight the significant large- and small-scale differences that appear between the two simulations due only to a change in the chosen cumulus parameterization. The overview describes the time between 12 and 72 hours into the simulation, encompassing that part of the simulation during and after the period of the track-split.

2) HELENE-GRELL

The evolution of the large-scale fields in the Grell simulation at the surface (Figs. 2.5 a, c, e, and g) and the PV and winds in the 348-to-351K isentropic layer (Figs. 2.5 b, d, f, and h) are quite similar to those in the analysis. The slowed progression of the central-Atlantic upper trough and its subsequent merger with the upstream upper-trough after 48 hours mirror

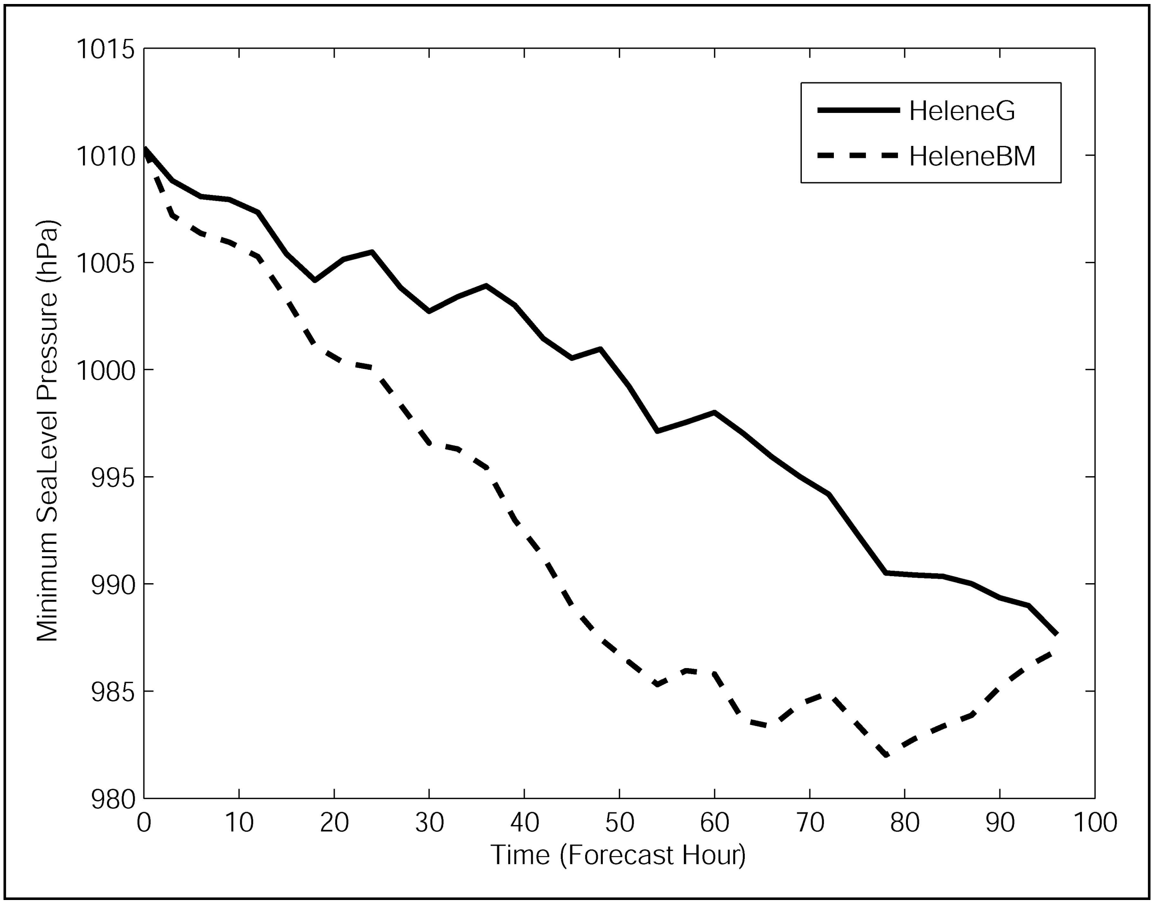

Figure 2.4. Time series of minimum sea level pressure for Helene-BM and Helene-G simulations.

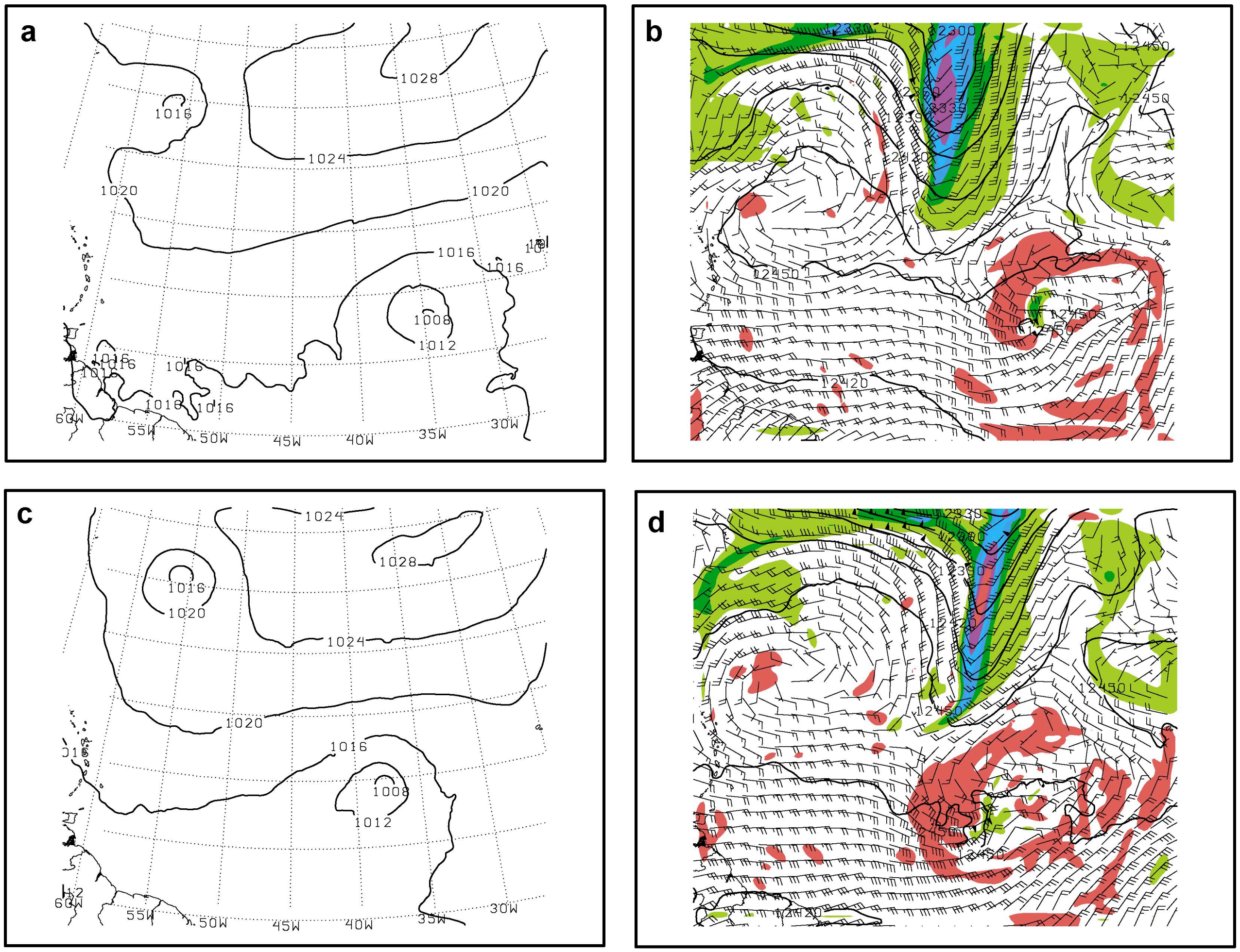

Figure 2.5. Mean sea level pressure and upper tropospheric PV in Helene-G simulation. PV is isentropic in 351-354 K layer. Geopotential height (200 hPa) contoured every 30 m. Winds plotted in ms^{-1}. Mean sea level pressure contoured every 4 hPa. Panels a and b correspond to 12 UTC 14 September 2008. Panels c and d correspond to 00 UTC 15

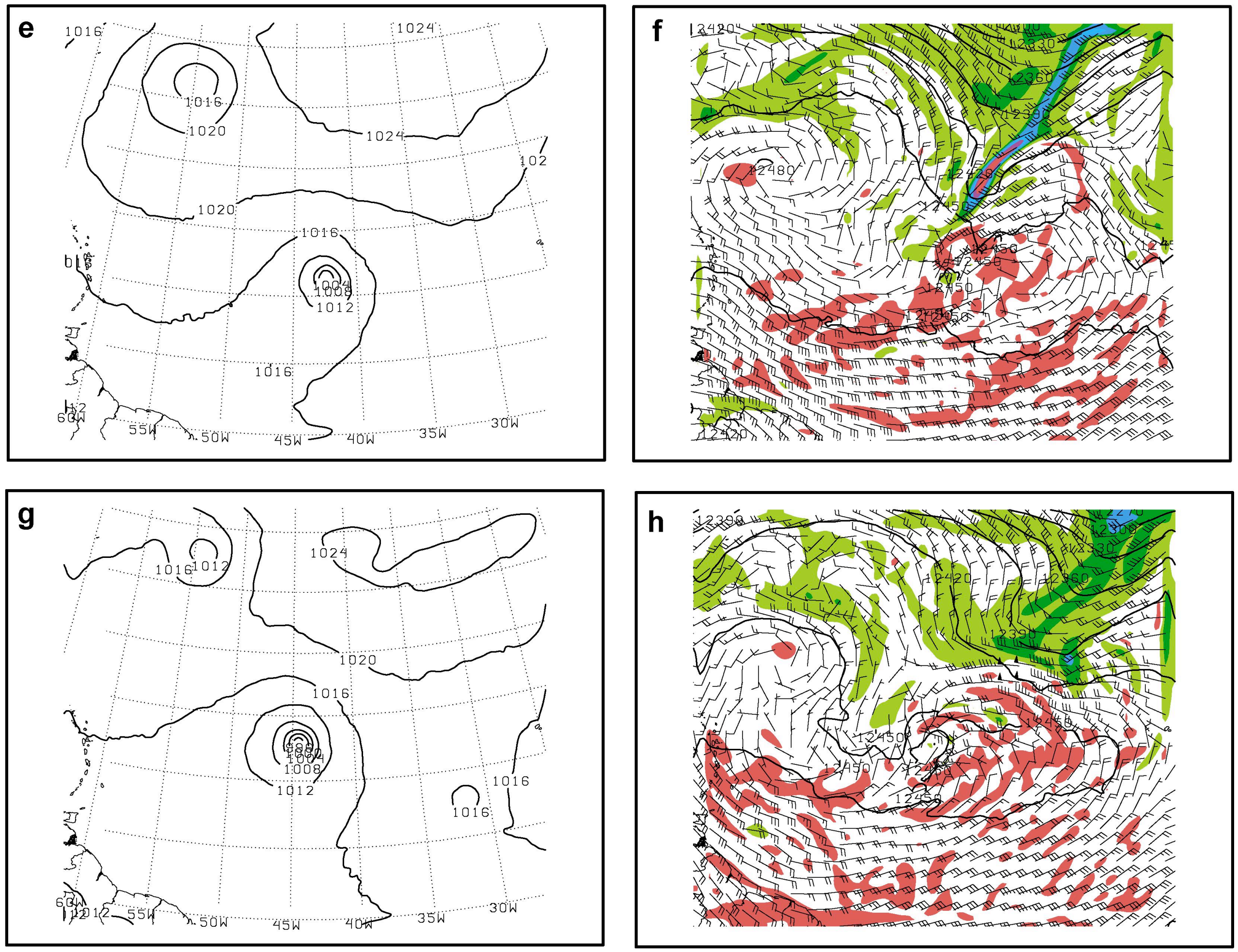

Figure 2.5. continued. Panels e and f correspond to 00 UTC 16 September 2008. Panels g and h correspond to 00 UTC 17 September 2008.

the sequence seen in the analyses. The upper tropospheric anticyclone in the Grell simulation appears to first build south- and eastward over the simulated TC during the first 24-hours of the simulation and then build over the TC as the TC intensifies. The upper trough to the north of Helene-Grell appears to advect most of the low PV TC outflow to the east of the center of Helene-Grell – contributing to the anticyclone's appearing to develop to the TC's east. The lack of appreciable advection of the low outflow PV to the north suggests that any direct interaction of Helene-G with the upper trough is limited in the first 36 to 48 hours of the simulation.

The Helene-G TC develops in an environment of moderate shear (Fig. 2.6). There are increases in the 850-300 hPa thickness over the center during the intensification of Helene-G.

3) HELENE-BM

During the first 12 hours of the simulation, Helene-BM had moved in a general westward direction, south of a subtropical ridge (Figs. 2.7 a and b). Over that same time interval, the 300-850 hPa thickness increased over the cyclone with shear over the cyclone remaining relatively weak (Fig. 2.8a). There are no obvious differences in the progression of the large-scale trough north of Helene-G and Helene-BM (Compare Figs. 2.5b with 2.7b). In contrast with the Grell run however low PV generated in the outflow of Helene-BM has been advected much further to the north of the modeled TC, forming a closed anticyclonic gyre north and east of Helene-BM, by 24 hours into the simulation (Fig 2.7d). During the subsequent 24 hours, ending at 0000 UTC 16 September, Helene-BM intensifies rapidly in an upper-tropospheric, low shear environment (Figs. 2.8 b and c). By 60 hours into the Betts-Miller simulation, large-scale differences in the upper-tropospheric outflow anticyclone are

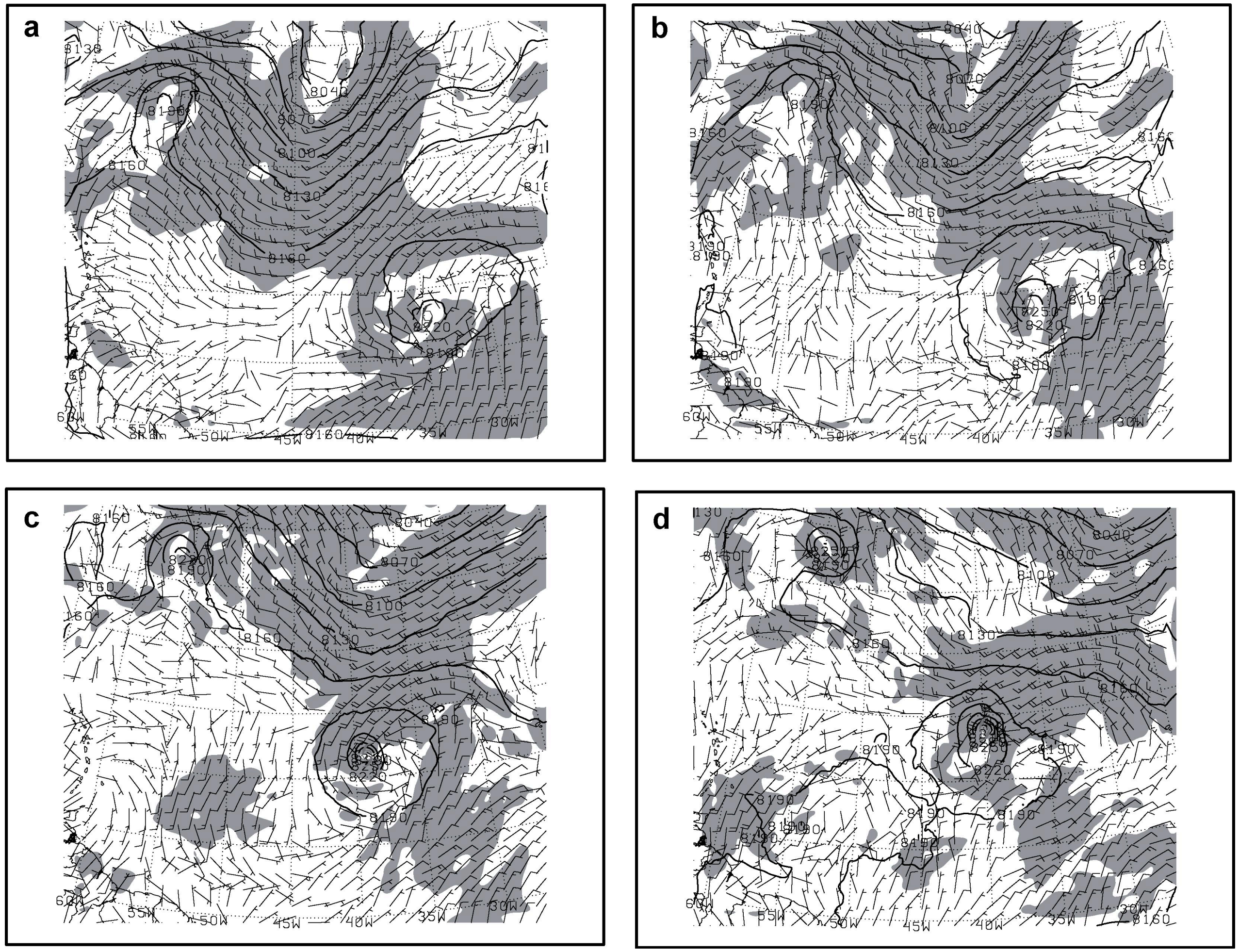

Figure 2.6. 850-300 hPa thickness contoured every 30m and shear vectors in ms^{-1} for the Helene-G simulation. Isotachs of shear vectors shaded. Panel a corresponds to 12 UTC 14 September 2008. Panel b corresponds to 00 UTC 15 September 2008. Panel c corresponds to 00 UTC 16 September 2008. Panel d corresponds to 00 UTC 17

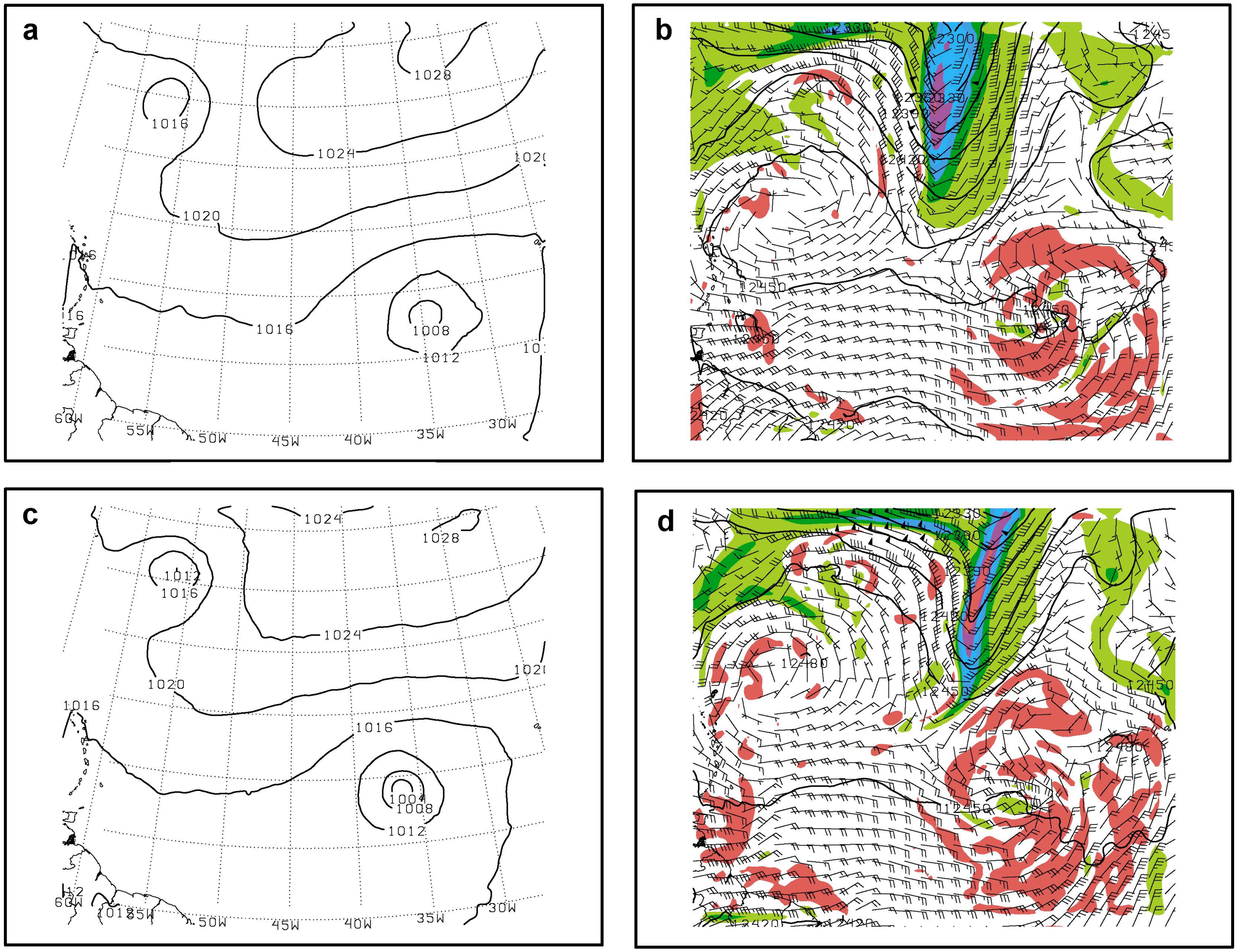

Figure 2.7. Mean sea level pressure and upper tropospheric PV in Helene-BM simulation. PV is isentropic in 351-354 K layer. Geopotential height (200 hPa) contoured every 30 m. Winds plotted in ms^{-1}. Mean sea level pressure contoured every 4 hPa. Panels a and b correspond to 12 UTC 14 September 2008. Panels c and d correspond to 00 UTC 15

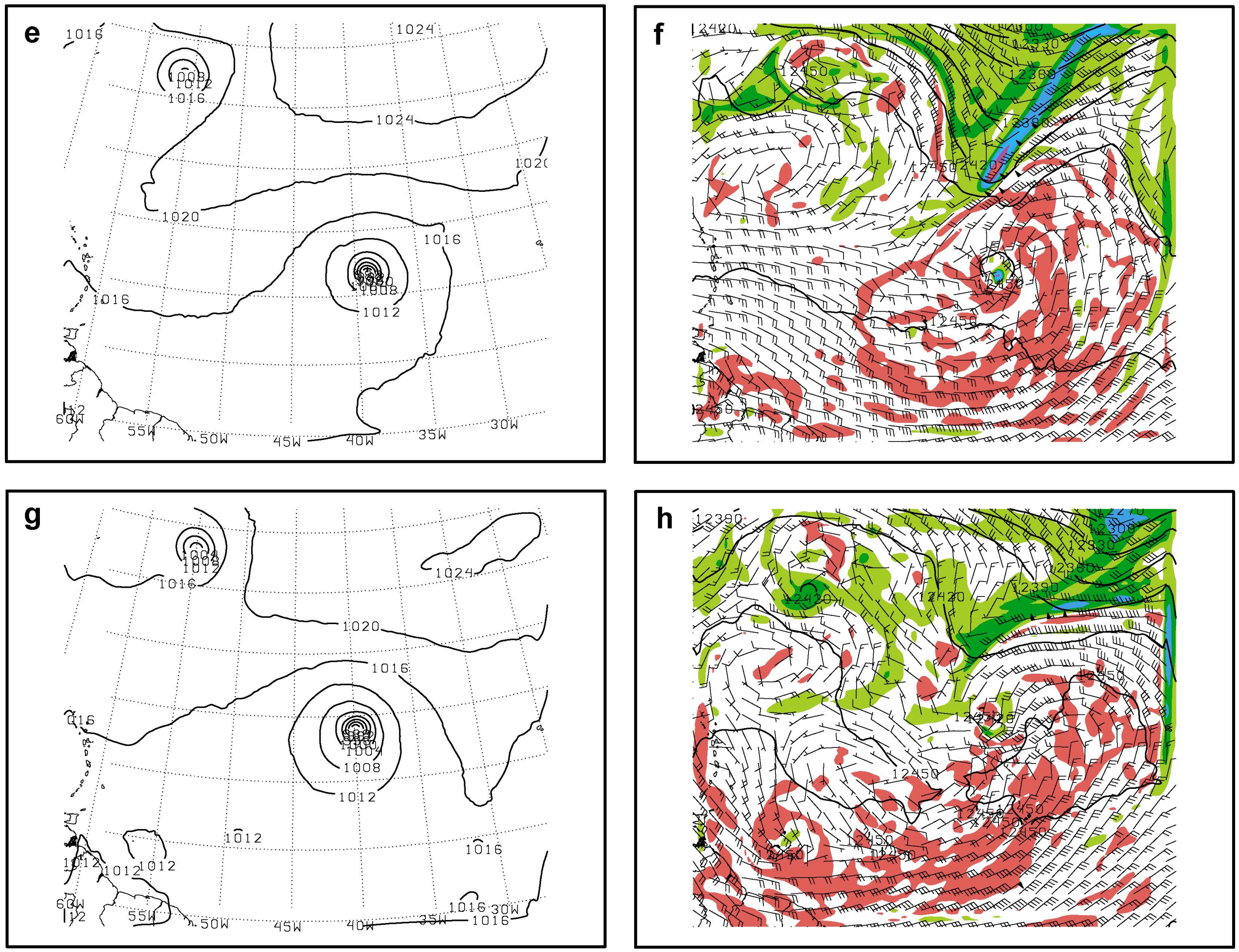

Figure 2.7 continued. Panels e and f correspond to 00 UTC 16 September 2008. Panels g and h correspond to 00 UTC 17 September 2008.

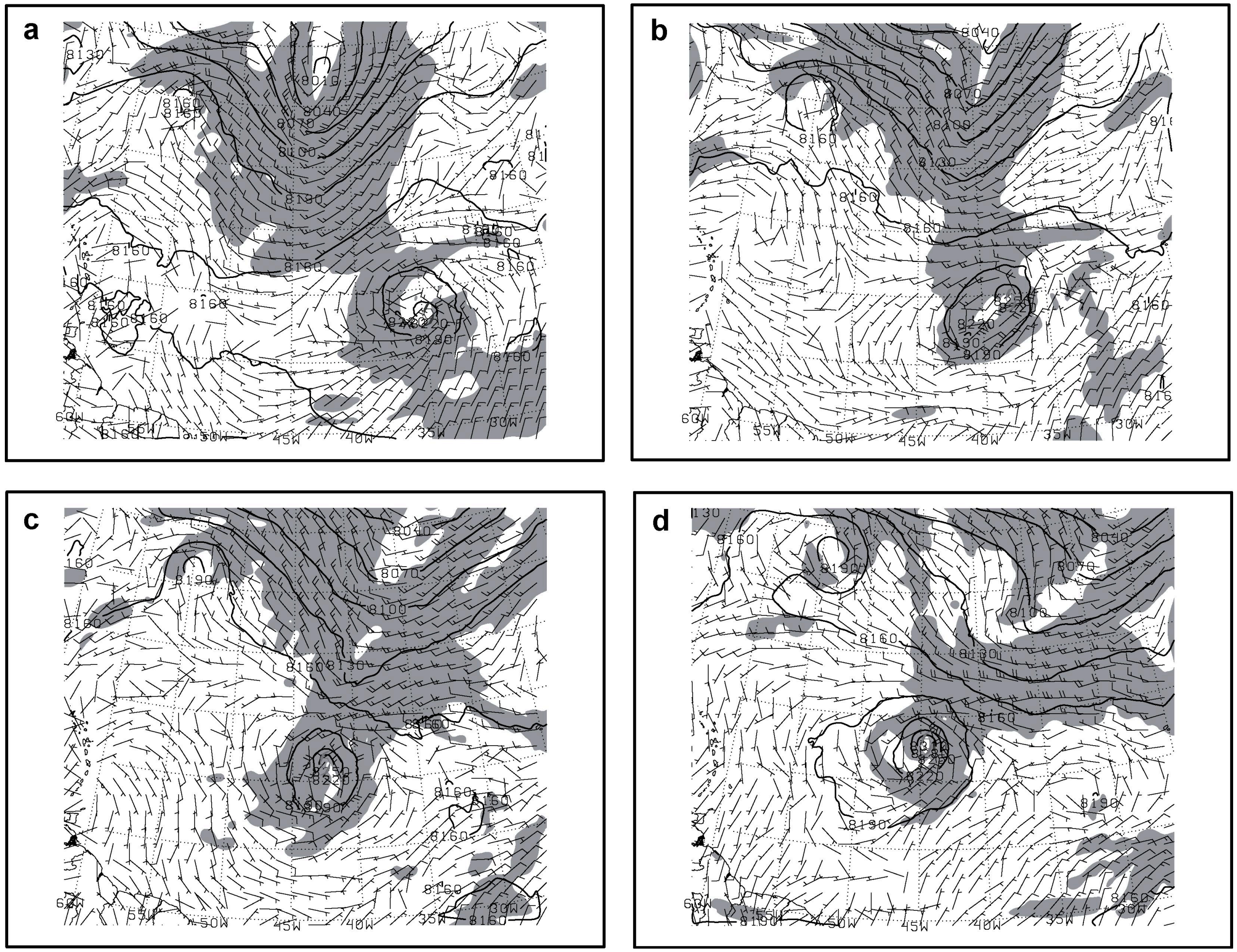

Figure 2.8. 850-300 hPa thickness contoured every 30m and shear vectors in ms^{-1} for the Helene-BM simulation. Isotachs of shear vectors shaded. Panel a corresponds to 12 UTC 14 September 2008. Panel b corresponds to 00 UTC 15 September 2008. Panel c corresponds to 00 UTC 16 September 2008. Panel d corresponds to 00 UTC 17

apparent. In particular, Helene-BM is nestled in a low PV large-scale anticyclonic gyre (Fig. 2.7f) while Helene-G is located to the west of a much less well-developed anticyclone (Fig. 2.5f). The shear becomes more significant after 60 hours corresponding to the time Helene-BM levels off in intensity. Subsequent increases in shear over center after 72 h (Fig. 2.8d) may herald demise of Helene-BM. Of importance to the discussion to follow is the transport and development of an area of relatively low upper-tropospheric PV to the immediate northeast, east and south of Helene-BM. By 72 hours, the large-scale differences between the two simulations have become more pronounced. The upper-trough to the northwest of the modeled TCs has had a much slower eastward and southward progression in the Betts-Miller simulation relative to the Grell simulation. While not the focus of this work, it is important to note that despite the differences in the handling of the other TC vortex in the northwest of the domain, both simulations had a relatively similar upper-tropospheric flow in the northwest quadrant of the domain. The similarities in this region were, in part, due to the boundary condition forcing.

Figure 2.9 shows the development of an area of positive geopotential height differences at 250 hPa between the BM and Grell simulations of Helene for the period F12 through F18. These height differences are consistent with a stronger flow out of the southeast at this level in the BM simulation relative to the Grell simulation. This height difference is seen during the time the track split initiates. While the height anomalies are modest, they occur at a relatively low latitude and could therefore represent a balanced flow of a few meters per second – sufficient to steer the simulated Helene northward relative to the observed and modeled track of the Grell simulation.

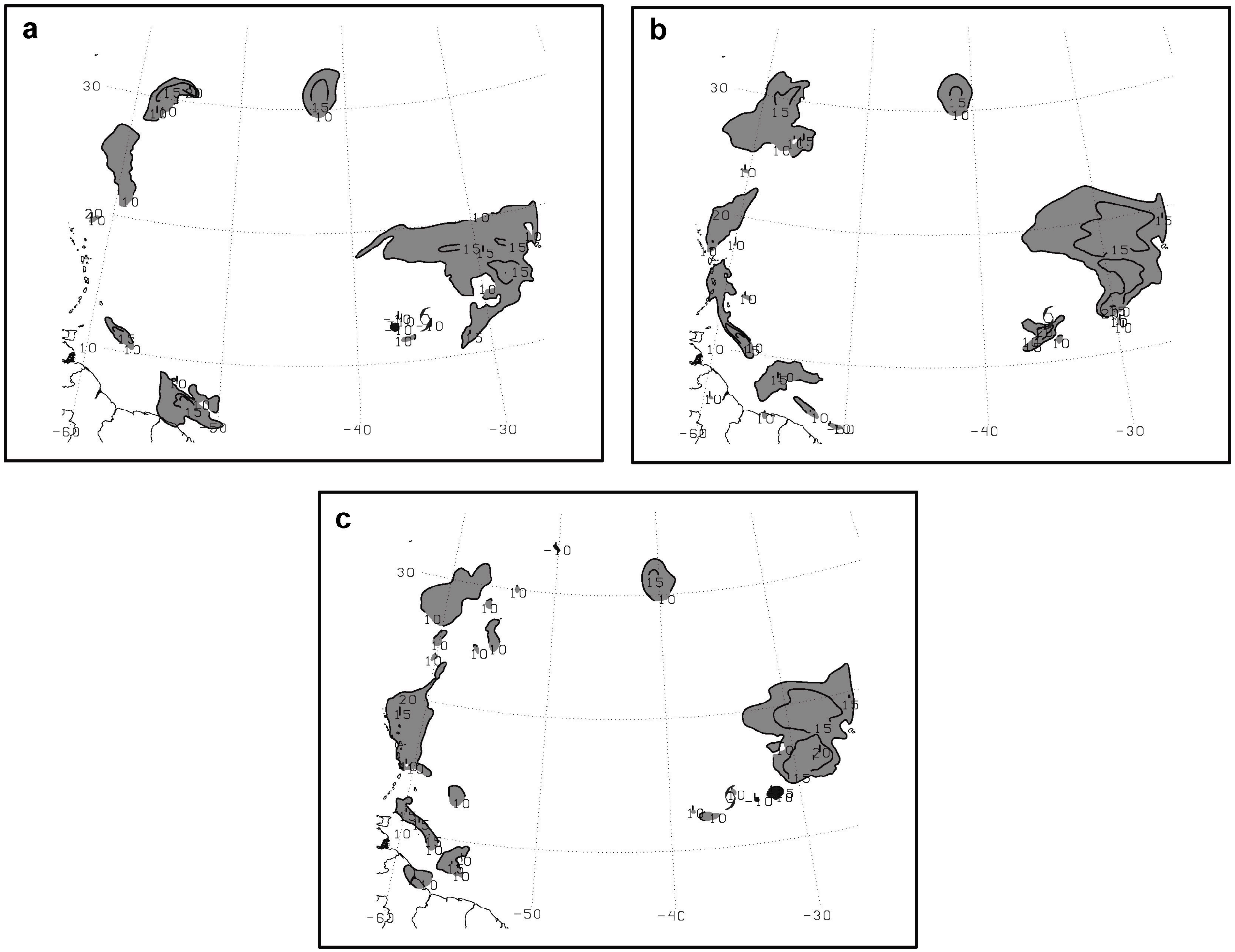

Figure 2.9. Differences in geopotential height between Helene-BM and Helene-G at 200 hPa for (a) 12 UTC, (b) 15 UTC, and (c) 18 UTC 14 September 2008. Positive values (indicating higher geopotential heights in the Helene-BM simulation) are shaded above 10 m.

While it is apparent that there are large-scale differences appearing in the upper-tropospheric flow, further diagnostics are required to determine whether these differences were responsible for the track split. We next describe the differences in the simulations' forecast of the tropical cyclone PV tower.

4) COMPARISON OF PV STRUCTURE OF SIMULATED TCS

In this subsection, we see that differences are apparent also at the TC scale. Figure 2.10 is a 12-panel plot comparison of north-to-south cross sections of the PV structure of Helene-BM (left panels) and Helene-G (right panels) just prior to and following the significant track split. Figures 2.10 a and b show that as early as 12h into the simulation, significant differences have developed. For Helene-BM, the meridional PV cross section reveals an upright PV tower with the PV maximized in the mid-troposphere, while for Helene-Grell, the PV values are small, located in the lower troposphere, and are not as compactly distributed .

A full day into the simulation, the TC PV differences become starker; the BM simulation (Fig. 2.10 c) reveals a robust, vertically erect PV tower, while the Grell simulation (Fig. 2.10d) exhibits a disorganized PV maximum in the lower troposphere. The values of PV are lower in the Grell simulation – consistent with a weaker TC.

By 36-42 hours into the simulation (Figs. 2.10e and 2.10g), the PV structure of Helene-BM presents the classic cyclonic PV tower described by Shapiro and Franklin (1995), Wu and Emanuel (1995a,b), Shapiro (1996), and Wu and Kurihara (1996). The PV in Helene-BM appears to be organized into a large maximum at mid-levels embedded in nearly uniform PV throughout the surrounding troposphere. Such a structure was described by Prater and Evans (2002) in their simulation of Hurricane Irene (1999) using the BM

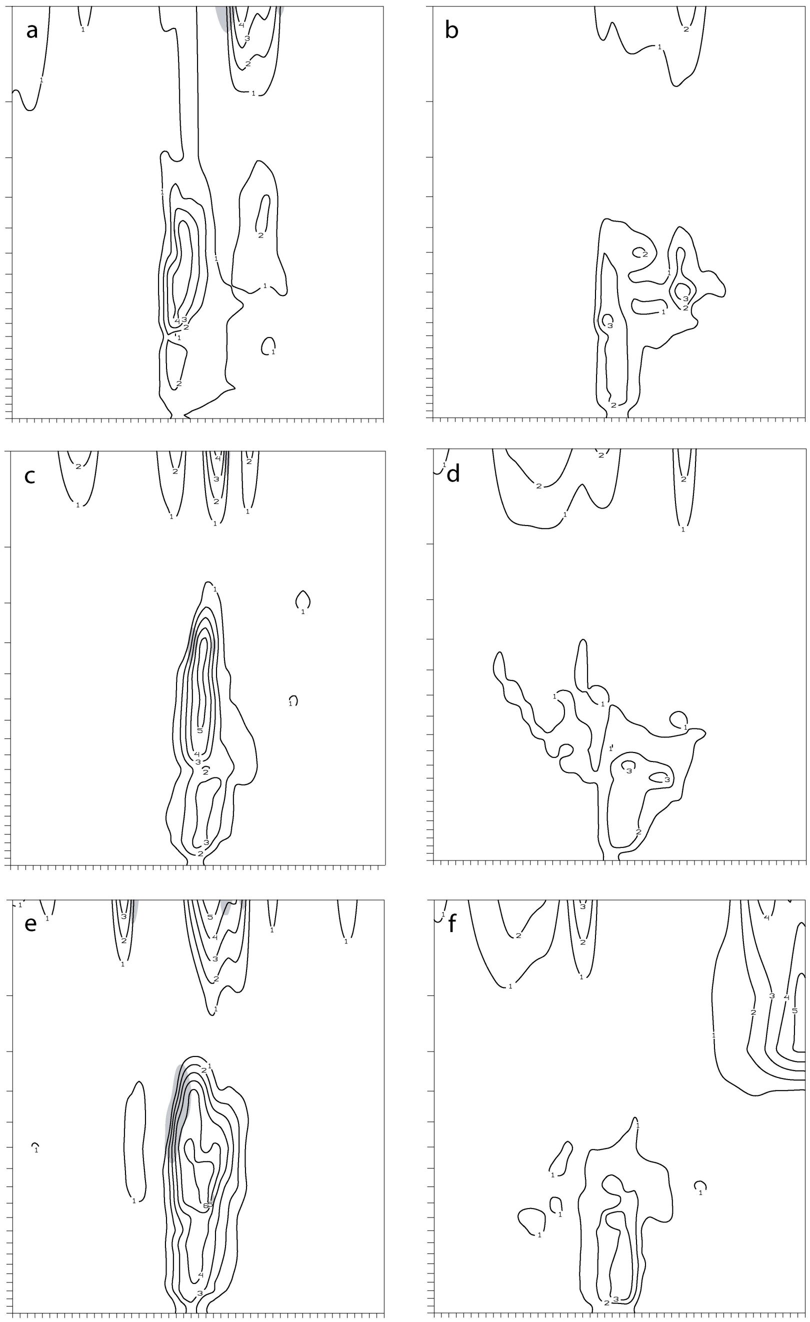

Figure 2.10. Potential vorticity (PV) cross sections taken north-south through the minimum sea-level pressure at 12 hours (panels a, b), 24 hours (panels c, d), and 36 hours (panels e, f) into the model simulation. The left (right) panels are valid for the Helene-BM (Helene-G) simulation. PV is contoured every 1 PVU, and the magnitude of the horizontal PV gradient is shaded for values between 7.0-8.0 x 10^{-11} $PVUm^{-1}$. The vertical axis is discretized by sigma levels.

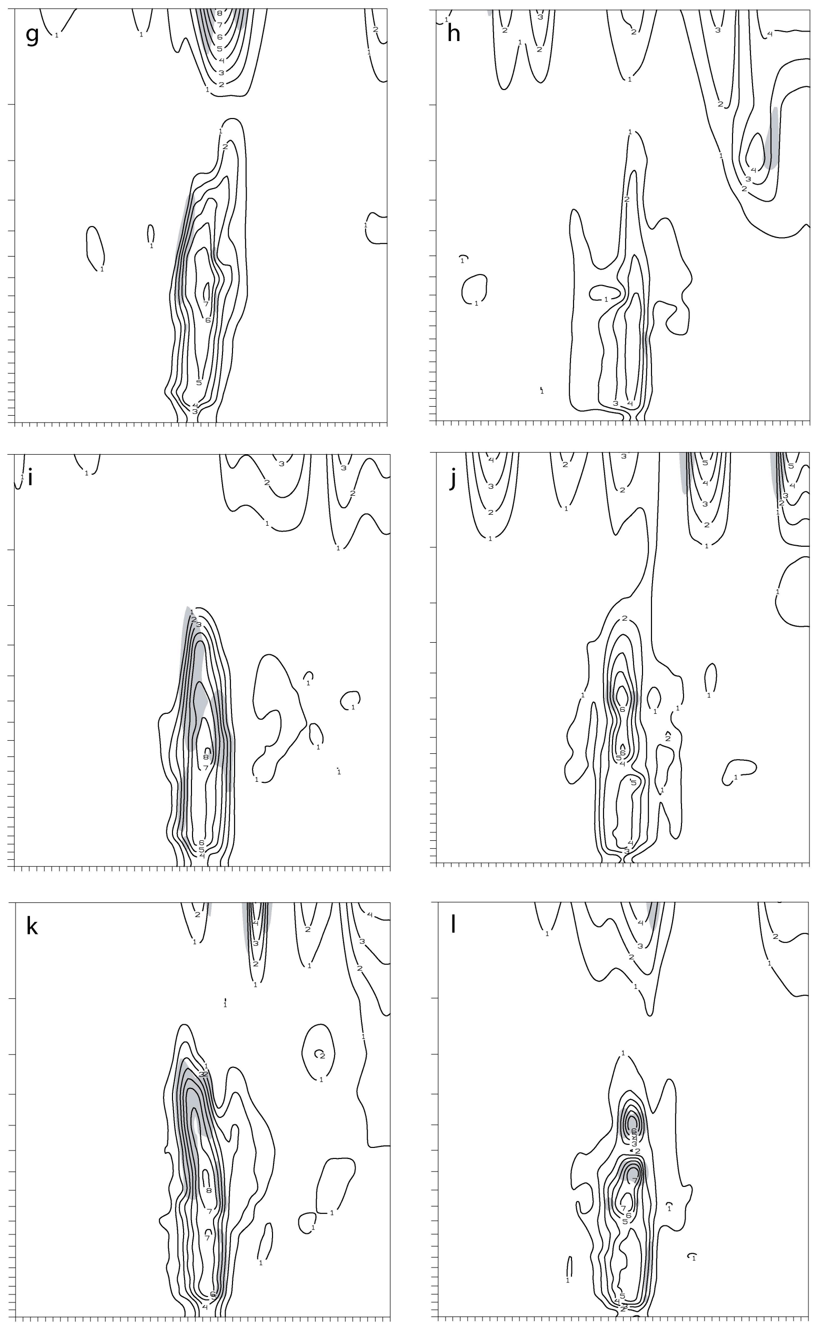

Figure 2.10 continued. Panels g and h correspond to 42 hours into the simulation. Panels i and j correspond to 60 hours. Panels k and l correspond to 84 hours.

scheme. Their study noted that the strongest heating rates were near 400 hPa in the core of their simulation of Irene when the BM scheme was used. They further noted that the profile observed in the simulation was consistent with previous studies of modeling tropical convection using the BM scheme (Betts and Miller, 1986; 1993). The location of the PV maximum in the BM simulation at this time is at the 450-400hPa level, consistent with heating profiles from these previous studies.

In Helene-G, at the same times (Figs. 2.10 f and h), the PV is distinctly weaker, maximized at a lower level, and the cyclonic PV tower is not as deep as in Helene-BM. Recall, at this time, there is also roughly a 10 hPa difference between the minimum sea level pressures of both simulations (Fig. 2.4). This is evidence of the VI-VD relationship in PV also found in the case study of Hurricane Bob (Wu and Kurihara 1996).

The basic structure of the Helene-BM PV (tower-like structure with maximum in the mid-troposphere) changes very little 60h into the simulation (Fig. 2.10i), with the exception being an increase in the surrounding PV gradient as the interior values increase. The structure of the Helene-G PV, however, does begin to exhibit notable changes (Fig. 2.10 j) as the maximum PV shifts from the lower-troposphere to mid-troposphere. In contrast with the BM simulation, the Grell simulation PV exhibits more discretely organized PV maxima.

5) DISCUSSION

It would seem that the VI-VD relationship described by Velden and Leslie (1991) and Wu and Kurihara (1996) holds for this set of simulations. The BM simulation, which reaches a greater maximum intensity as measured by MSLP, also appears to exert a stronger influence on and is influenced more strongly by a passing upper-level trough. The Grell simulation, which remains weaker than the BM simulation throughout the entire simulation, appears to be influenced far less by the synoptic features at upper levels because the cyclonic vortex (and the outflow at the top of it) which characterizes the TC structure is not tall enough to feel the effects of the passing upper trough as strongly as in the BM simulation.

However, several questions have yet to be answered. First of all, if the difference between the two tracks can be attributed to a difference in vortex-depth (related to a difference in vortex intensity), then why did the track-split occur around F18, when there was only a 3 hPa difference between the two simulations? Secondly, is the greater influence of the upper trough in the BM simulation apparent in the structure of the optimal steering column? Finally, what relationship if any exists between the structure of the optimal steering column and the TC structure beyond a simple VI-VD relationship? These unanswered questions are at the core of this study.

As suggested by Prater and Evans (2002), once two simulations significantly diverge from one another they may eventually move into significantly different environments which further change the modeled TC's structure and steering. For that reason, this study separates the simulations into two time periods: (1) the time period surrounding the track-split between two simulations of the same TC, and (2) beyond that time, when the two simulations can largely be considered to be two separate cases evolving in two separate environments, and a consistent relationship between PV structure and steering column depth will be sought for both cases.

2.3 Methodology

The relationship of the structure of the optimum steering column (specifically, the vertical extent of the averaging domain as well as where that domain is centered in the vertical) will be compared to the PV structure of the modeled TC. As the PV structure of the TC evolves, we expect that the vertical extent and vertical placement of the optimal steering column will likewise evolve. First, we will calculate PV on the model's native vertical coordinate. This PV will be used to define significant vertical levels at which we expect significant PV advection, and therefore we expect the optimal steering column to be centered at those locations.

The calculation of the steering from any steering column is a simple task. Given the dimensions of the averaging box, the vertical depth of the box, and the location of that box in the model, the winds are averaged to remove the symmetric component of the flow associated with the TC vortex. The remaining flow is assumed to be the environmental flow which advects the TC PV and steers the TC. For a steering column of any given dimensions and location within the model, a steering cost function can be defined which computes the difference between the steering calculated from the averaging done within the steering column to the actual motion of the storm. A high steering cost function indicates that the calculated steering deviates strongly from the actual motion of the storm, indicating poor performance. The dimensions and location of the averaging box which provides the lowest steering cost function defines the optimal steering column.

a) Calculation of potential vorticity

The calculations performed in this study are done in the MM5's native vertical coordinate, σ, defined as:

$$\sigma = \frac{p - p_T}{p_s - p_T}$$

where p is the ambient pressure, p_T is the pressure at the top of the model (set to 50 hPa for this study), and p_s is the reference-state surface pressure. The PV used in this study is an approximation to the full Ertel PV $q = \frac{1}{\rho}\vec{\omega}_a \cdot \nabla\theta$, wherein the hydrostatic approximation has been made and vertical-motion terms neglected:

$$q \cong -g\frac{\partial\sigma}{\partial p}\frac{\partial\theta}{\partial\sigma}\left(f + \frac{\partial v}{\partial x} - \frac{\partial u}{\partial y}\right) + g\frac{\partial\sigma}{\partial p}\left(\frac{\partial\theta}{\partial x}\frac{\partial v}{\partial\sigma} - \frac{\partial\theta}{\partial y}\frac{\partial u}{\partial\sigma}\right)$$

where u and v are the zonal and meridional velocity components, ρ is the density, $\vec{\omega}_a$ is absolute vorticity, and θ is the potential temperature. Ertel PV is calculated at cross-points on half-sigma levels.

b) Calculation of PV maximum, PV "center of mass", vorticity maximum, and vorticity "center of mass"

Once the steering and cost-function of each steering column is calculated, the relationship between the TC steering and the TC structure can be evaluated. For this study, we are interested in four vertical levels of the TC for their significance to TC steering from a vortex-advection perspective.

First, we wish to look at the steering of the TC with respect to the height of its PV maximum. At this level, provided the TC is in a homogeneous environment, it is argued, the horizontal gradients of PV will be the strongest, and thus the largest contribution to TC steering should come from advection of PV at this level. Therefore, we would expect that the characteristic error of a steering column should be minimized when the column is centered about the level of the PV maximum in the TC. Secondly, we wish to look at the steering of the TC with respect to the vertical level of a PV "center of mass". This level may be thought of as a significant level for advection given the aggregate effect of PV advection throughout the depth of the TC's entire cyclonic PV tower. The last two levels of interest are the vorticity analogs to these two regions, the level of the vorticity maximum of the TC and the level of the vorticity "center of mass" for the TC.

The process for calculating these levels is simple. The TC vortex is taken to encompass any region of the TC where the ambient vorticity is greater than 1.7 x $10^{-4}s^{-1}$. This is to ensure that PV attributed to high stratification in the lower stratosphere does not enter into the computations for the vertical level of the PV maximum and PV center of mass. An average of vorticity over 25 grid points centered on the TC MSLP is calculated at each level and evaluated against the threshold vorticity value of 1.7 x $10^{-4}s^{-1}$. The top of the TC vortex tower is defined as the level at which this average vorticity goes below the threshold value.

Once the top of the TC PV tower is specified, the PV calculated within the steering column box, centered on the MSLP of the TC, is scanned for its highest value. The vertical level at which this maximum is found is recorded as the level of the PV maximum for that time. The calculation of the PV center of mass involves adding up all of the PV in the box underneath the defined PV tower top, and performing a "center of mass" calculation, treating PV like a density function in space:

$$q_{COM} = \frac{\sum_{k=bot}^{top} k\, q_k}{\sum_{k=bot}^{top} q_k}$$

where the summation takes place over vertical levels (k) from the bottom of the tower to the top as defined above. Here, q_k refers to the total PV on a particular vertical level (k), and the summation is over the entire volume comprising the TC cyclonic PV tower. It is important to remember that q is calculated on *half-sigma* levels. We take the value of PV at a half-sigma value to represent the PV in the two full-sigma level layer surrounding it.

The vertical level of the vorticity maximum and the vorticity center of mass are also calculated using the procedure described above applied to the three-dimensional vorticity rather than the PV. Vorticity is interpolated to half-sigma levels in order to maintain the consistency of the analysis with respect to both the PV and vorticity fields.

c) Calculation of steering from steering columns

At any time, the "observed" motion of a simulated TC, defines a Modeled Hurricane Motion Vector (MHMV) with zonal and meridional components u_m and v_{m} respectively, calculated by averaging the motion of the MSLP over the six hours centered on that time. Output from the simulations is on 20 equally spaced half-sigma levels, from 0.975 nearest the surface, up to 0.025. We define a *steering column* as a column depth over which the horizontally averaged winds are vertically averaged to calculate a possible steering flow. Since the sigma levels are equally spaced, mass-weighted steering columns can be calculated by performing simple averages. Every 3-h, a number of steering columns are calculated by performing a horizontal and vertical averaging of the winds surrounding the TC. The horizontal average is performed on a box centered on the MSLP minimum, with a fixed horizontal extent chosen as 51 x 51 grid points. Averaged winds for the steering columns are calculated for every possible steering column-depth and vertical position of that steering column. Since there are 20 vertical levels, there are 20 vertical positions for a steering column one level deep, 19 vertical positions for a steering column two levels, deep, and so on. Thus, a total of 210 steering columns are analyzed at each time.

The estimated motion from a steering column can be evaluated against the MHMV by use of a cost function:

$$J = \sqrt{((u_s - u_m)^2 + (v_s - v_m)^2)}$$

where u_s and v_s are, respectively, the zonal and meridional components of the horizontally and vertically averaged horizontal flow surrounding the TC as estimated by a steering column. The cost function represents the length of the vector difference between the estimated motion of the TC by a steering column and the observed MHMV.

There are essentially three pieces of information which must be evaluated when analyzing the performance of a steering column. The first two define the characteristics of the column itself – the vertical extent of the steering column and the center location of the column in the vertical. Because all of the steering columns use the same horizontal dimensions, it is these criteria which define the unique characteristics of a given steering column. A steering column may be thin, only encompassing a few layers of the model, or deep, encompassing many or all of the layers. Likewise, a steering column may perform an average over the lower levels of the model, or only the middle layers, or only the uppermost layers. Thirdly, the performance of that steering column is an important piece of information. The steering cost function, J, is used to define the accuracy of a steering column by comparing the calculated steering of the TC to the observed motion of the TC through use of the MHMV. A high cost function value indicates poor performance of the steering column to diagnose TC motion.

In the following analysis, these three pieces of information: the depth of the steering column, the location of the steering column in the vertical, and the accuracy of the steering column, are presented in a single plot which allows the user to relate these characteristics of the steering column to the PV structure of the modeled TC through the four levels of interest described above.

2.4 Analysis

a) "Steering plots"

In this section, modeled TC steering is analyzed using "steering plots", which plot the steering cost function defined in the previous section as a function of the vertical level at which a particular steering column is centered. The abscissa is the model vertical level at which a steering column is centered, ranging from nearly the top of the model (0.025-sigma) to nearly the bottom (0.975-sigma). An example of such a plot is shown in Fig. 2.11 for the Helene-BM simulation at F18. Points corresponding to steering columns of the same vertical depth are connected and plotted as a curve with a particular color ranging from blue to orange indicating a change from thinnest to thickest steering columns. The construction of such a plot from a series of such points is presented in Fig. 2.11a-d. The four levels of interest, the centers of mass for vorticity and PV and the locations of the maxima in vorticity and PV are indicated just below the sigma-level labels by a square (PV maximum), circle (PV center of mass), cross (vorticity maximum), and triangle (vorticity center of mass) in Fig. 2.11e. Since there is a 0.05-σ difference between each vertical level, these four regions of interest, calculated on half-sigma levels, are considered to encompass a layer of 0.05-σ depth centered on their calculated vertical position. Assuming that the steering is the only

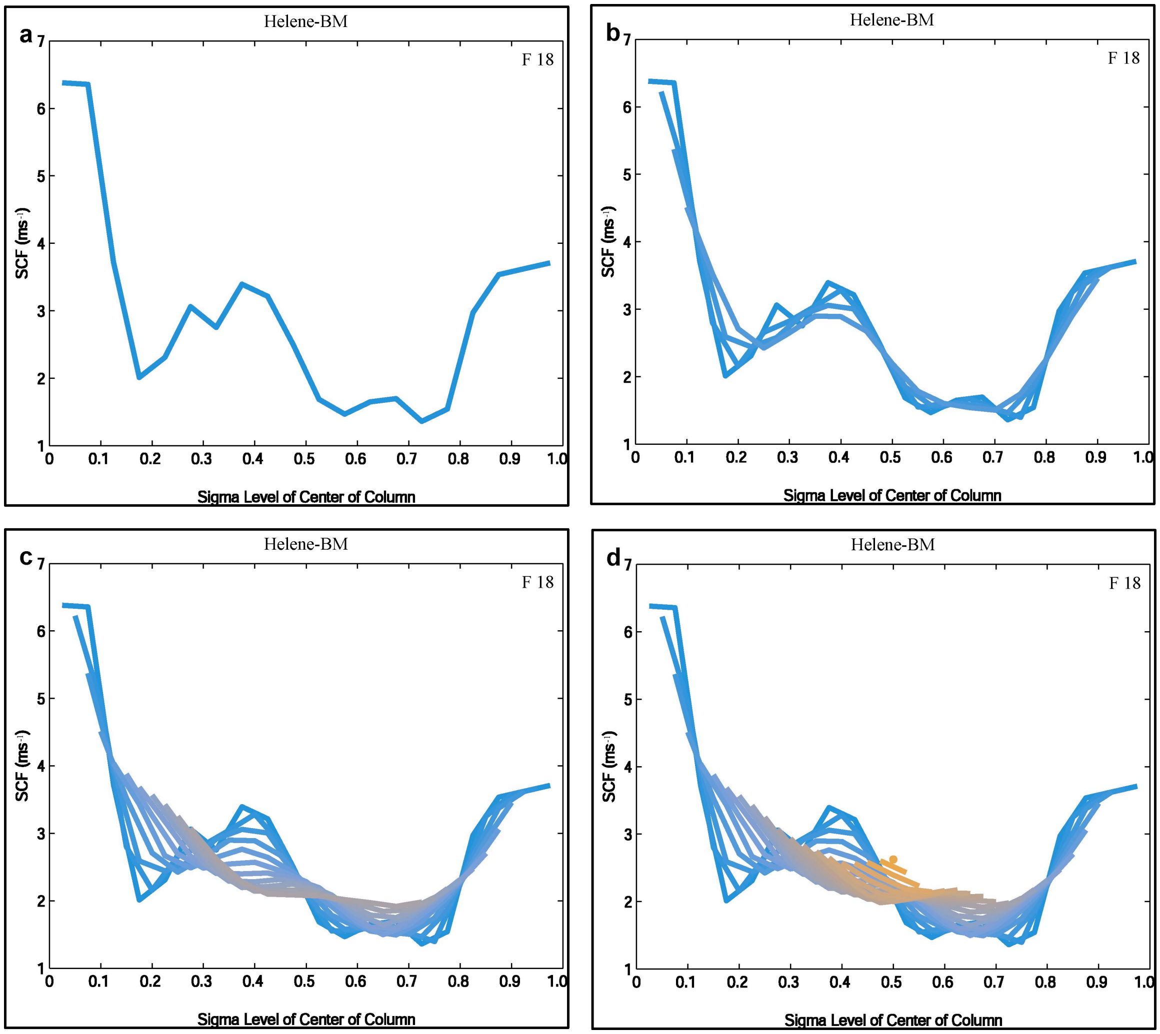

Figure 2.11. Four-panel plot describing the creation of a sample steering plot. Panel a shows a single line; each point along the line represents a one-level deep steering column. The vertical level of the column (center) is represented by the location of the point on the abscissa, ranging from the top of the model on the far left of the abscissa, to the bottom of the model on the far right. The accuracy of the steering column is represented by the location of the point on the ordinate. This is the value of the cost function (J); a high value indicates a large difference between the diagnosed steering from the steering column and the observed motion of the storm. Panel b shows the addition of two, three, and four level deep steering columns. Panel c shows the addition of even deeper steering columns; the color of the lines begins to change to represent the change from thin (blue) columns to deep (orange) columns. Panel d shows all steering columns used in the analysis.

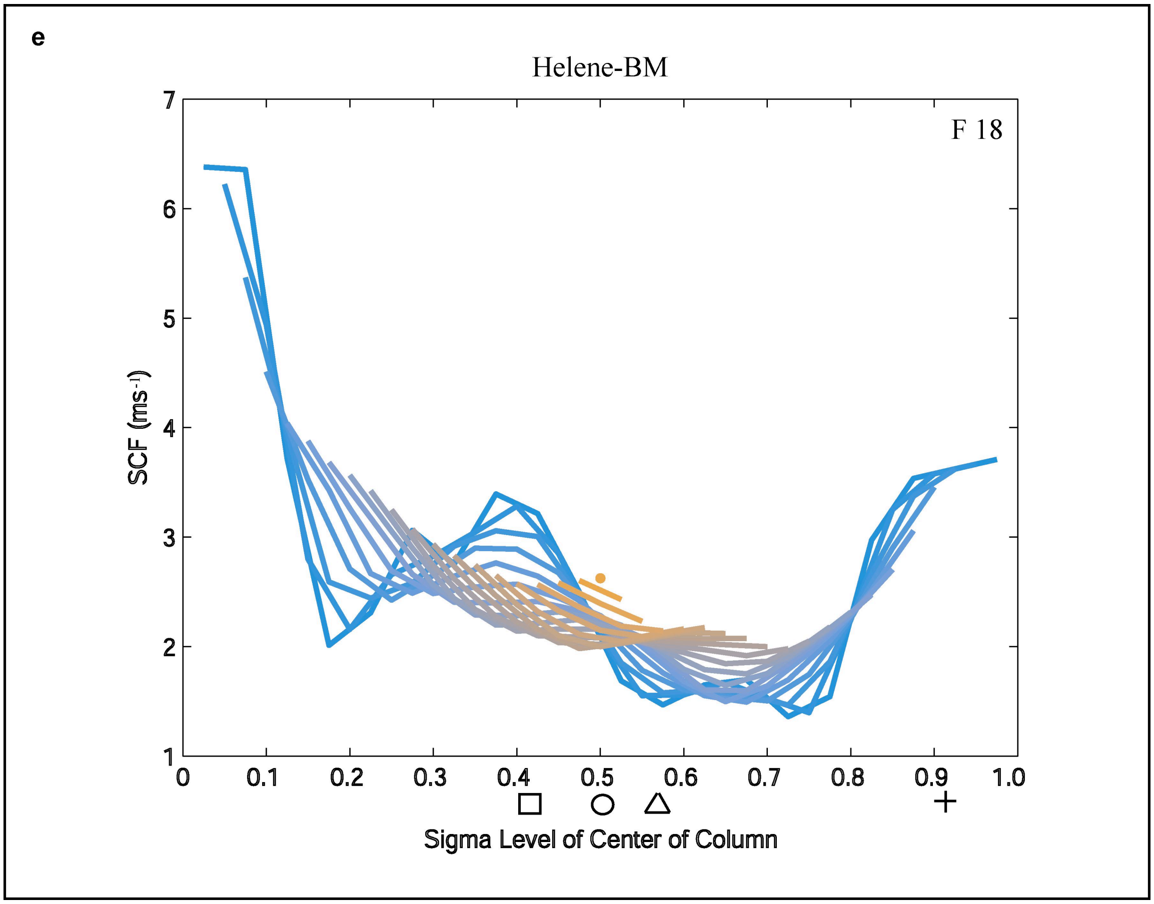

Figure 2.11 continued. Panel e is a completed steering plot for the Helene-BM simulation at 18 hours into the model simulation (F18). Four symbols along the abscissa correspond to the vertical level of the PC maximum (□), the vertical level of the PV center of mass (○), the vertical level of the vorticity maximum (+), and the vertical level of the vorticity center of mass (Δ).

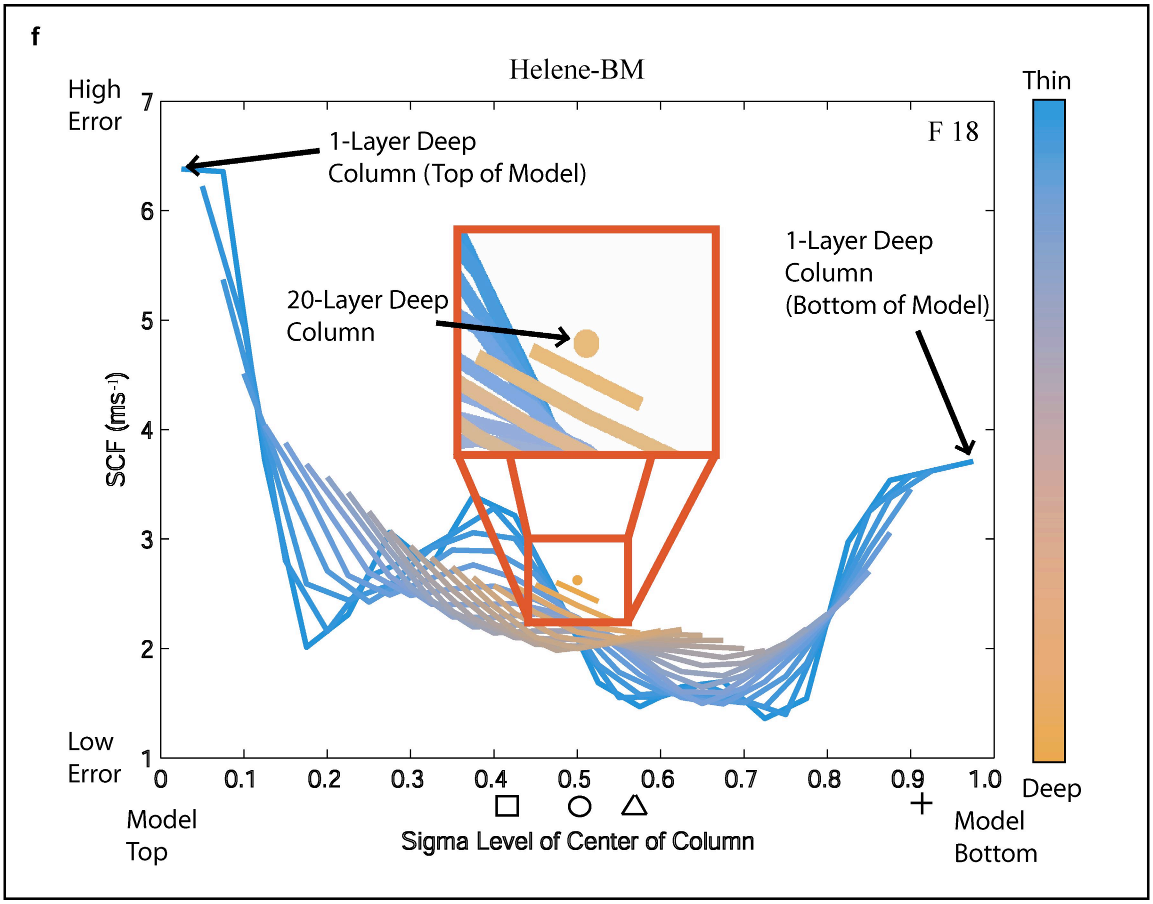

Figure 2.11 continued. Panel f is a deconstruction of the completed steering plot in Panel e. Points corresponding to the 1-layer deep column at the top of the model, the 1-layer deep column at the bottom of the model, and the full 20-layer deep column are labeled. The color bar on the right corresponds to the color of the lines indicating the depth of any steering column along that line.

mechanism governing TC motion, if the cost function is minimized for columns centered at a particular level, one can assume that this level is the steering level for the TC. A deconstruction of this plot is provided in Fig. 2.11f for further emphasis. The purpose of these plots is to show the relationship between the depth and vertical position of the optimal steering column to the structure of the TC PV and vorticity. A similar experiment was performed by Ueno (2003), in which an optimal weighting function was derived to describe TC motion in terms of weighted steering at each level. However, in Ueno (2003), TC motion was related to the sea-pressure tendency equation rather than the PV tendency equation.

Figure 2.11 is valid for the BM simulation at F18. The MHMV at this time indicates that the TC is moving 4.51 ms^{-1} to the west and 3.87 ms^{-1} to the north. A minimum in steering cost function appears in all steering columns centered about the vorticity center of mass, which at this time is at roughly the 700-to-750 hPa level (not shown). The steering cost function appears highest in steering columns centered at upper levels, and continually decreases as the center of the steering column is moved closer to the vorticity center of mass. In addition, the steering appears to slightly favor thin steering columns over thick ones (darker blue curves are lower on the ordinate, indicating lower values for the cost function, *J*).

From this example plot, it is clear that the steering plot is capable of revealing considerable information about all possible steering columns. This sort of analysis was performed at six hour intervals between F18 and F84 for both simulations to see if any consistent trends appear between the optimal steering column structure (depth and position in the vertical) and the corresponding TC vorticity and PV structure. Using these plots, the steering of both simulations will be analyzed and compared to their corresponding TC PV structure. The analysis will begin at a time period after the initial track split, and both simulations will be treated as isolated cases from which a single, consistent theory can be drawn which relates the optimal steering column structure to the TC PV structure. Once this has been done, and use of the steering plots has become familiar, the analysis will focus on the track split itself to identify significant differences in behavior of the two TCs, and how they are (or are not) visible in the steering plots.

b) Analysis

Figure 2.12 is a six-panel plot of steering plots for the Helene-BM simulation (left panels) and Helene-G simulation (right panels) at various times throughout the simulation. Over time, the steering in both simulations appears to be related to TC PV structure through three distinct relationships, or "steering regimes" defined by the level at which the optimal steering column is centered.

In "regime 1", represented by Figs. 2.12 a and 2.12b, it is apparent that the steering cost function can be minimized by centering a steering column at or near the location of the PV maximum. At F42, a minimum in steering cost function occurs in steering columns centered near the PV maximum. The PV maximum is found at roughly the 400 hPa level in the Helene-BM simulation, and slightly lower down in the Helene-G simulation, at about 450 hPa. Steering cost function appears to be minimized when a steering column is centered near the PV center of mass; however minimization of the cost function appears to be restricted only to thin columns (blue lines) in Helene-BM, while in Helene-G all steering columns are optimized at this level regardless of depth. Also, comparable minimization of the steering

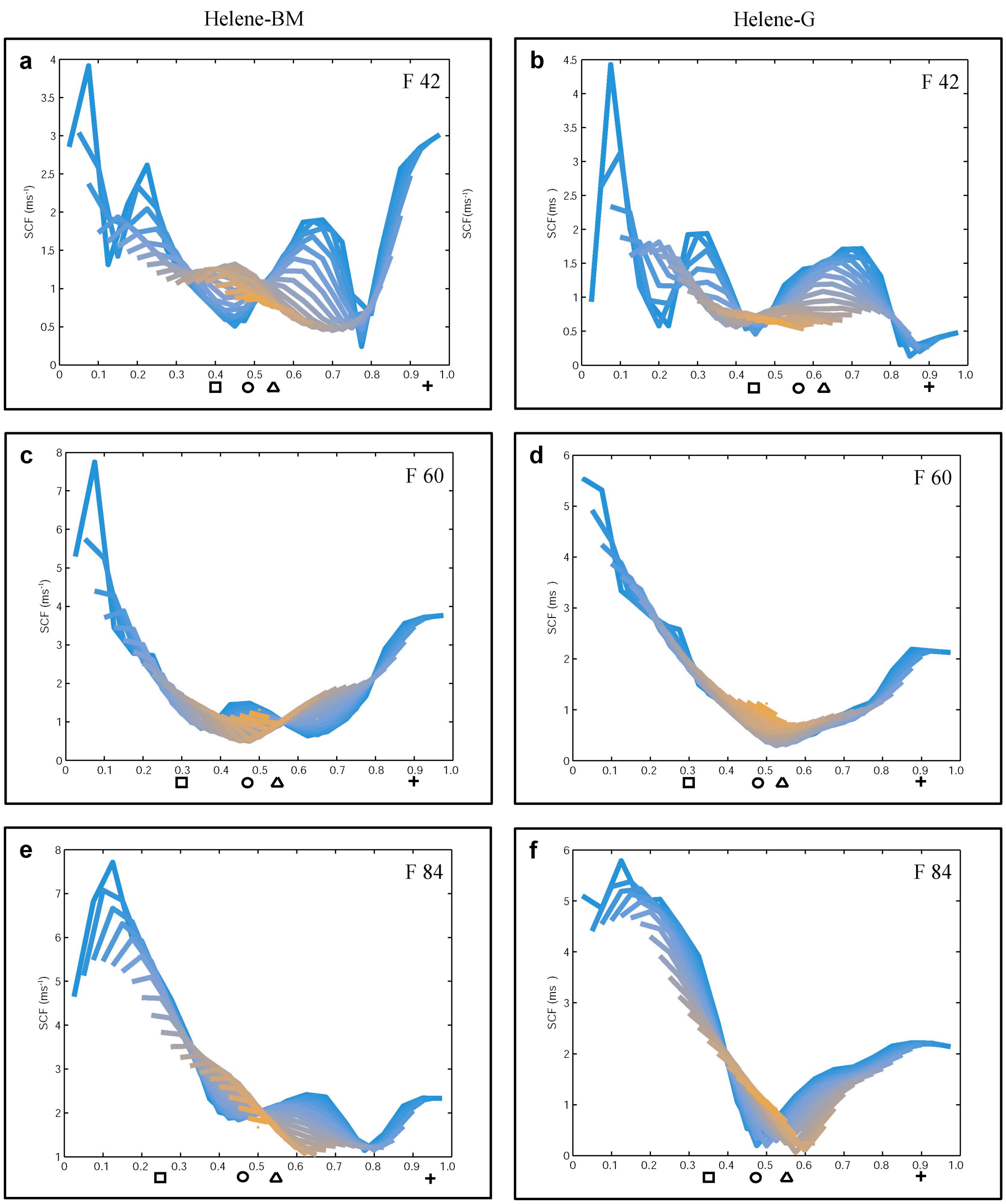

Figure 2.12. Steering plots (see Fig. 2.11) for the Helene-BM (left panels) and Helene-G (right panels) simulations for 42 hours (panels a and b), 60 hours (panels c and d), and 84 hours (panels e and f) into the model simulation.

cost function at earlier times can be achieved by performing an average over a thin steering column centered about a low level (roughly the 880 hPa level for Helene-BM, and 860 hPa for Helene-G), though neither of these locations coincides well with any of the levels of interest.

The steering characteristics of “regime 2” are represented by Figs. 2.12 c and d. At this time, the dominance of the PV maximum on steering begins to wane while the steering begins to be more sensitive to the PV center of mass and vorticity center of mass. In Helene-BM, the steering cost function appears to be minimized in the location of the PV maximum (~315 hPa) over thin columns, but in deeper columns the steering cost function is minimized at lower levels, at the level of the PV center of mass (~500 hPa). Equally low steering cost function can be accomplished by performing an average over a thin layer centered on the vorticity center of mass (~600 hPa). The steering cost function is bound between 0.7 ms^{-1} and 1.5 ms^{-1} in any column centered on the PV center of mass – which is within the error of the estimate of the magnitude of the MHMV.

The steering plot for Helene-G at the same time (Fig. 2.12d) shows a clear, single steering cost function minimum at the level of the PV center of mass (~500 hPa). The level of the PV maximum appears to be completely irrelevant to the motion of Helene-G at this time in the simulation. This minimum in steering cost function is independent of column depth, much like the minimum in steering cost function for Helene-G in regime 1. One might expect that little dependence of steering flow on column depth is an indication of low environmental shear, but the relationship is more complex. The implications for this depth-independence with respect to environmental shear will be discussed below.

A clear structure to the steering cost function curves has developed in "regime 3", represented by Figs. 2.12 e and f. In Helene-BM, the steering cost function minimum is clearly split between thin columns and deep columns. Thin columns appear to be minimized near the level of the PV center of mass (~500 hPa), and steering cost function increases with increasing column depth. Deep columns are minimized at the level of the vorticity center of mass (~600 hPa) and steering cost function increases with decreasing column depth. A (potentially spurious) minimum in steering cost function appears at the 0.8-sigma level which does not correlate with any of the four levels of interest. The PV maximum appears to be completely irrelevant to steering.

The same relationship can be seen in the Helene-G simulation at this time. Two distinct minima in steering cost function appear, each corresponding to either the PV center of mass or the vorticity center of mass. These minima are related to the depth of the steering column in the same way as in Helene-BM. Again, the level of the PV maximum is no longer relevant to the steering level.

c) Remarks

There is evidence to suggest that the steering of the modeled TCs is being consistently influenced by its PV structure. Moreover, the relationship observed between TC PV structure and steering column structure is more complicated than a simple relationship between vortex intensity and vortex depth. While the VI-VD relationship obviously cannot be dismissed or ignored, it is possible that the VI-VD relationship is an illustration of a more complicated relationship generalized over a vast number of cases with a broad range of intensities.

For these simulations, TC steering appears to be related to PV structure through three steering regimes. In regime 1, the TC is steered at the level of the PV maximum, though the accuracy of a steering column centered on or near that level is not necessarily dependant upon the depth of that column. In regime 2, there is a transition wherein the steering level moves from the PV maximum to the PV center of mass. Finally, in regime 3 a distinct pattern emerges where two minima appear in the steering plot; the optimal steering column is either a thin column centered on the PV center of mass, or a deep column centered on the vorticity center of mass.

In the next section, the PV structure of the modeled TCs will be analyzed at the same times corresponding to regime 1, regime 2, and regime 3 steering to relate the evolution of the optimal steering column structure to the evolution of the TC PV. In the preceding section, the relationship of the optimal steering column structure in regime 3 will be compared to the VI-VD relationship.

d) Relationship of steering to TC PV structure

The next step is to relate the observations of steering characteristics in the previous section to the vertical structure of the TC and the evolution of that structure throughout the simulation. In particular, we wish to understand why the optimal steering column appears to shift from being nearly located with the PV maximum to being located near the level of the PV center of mass. Such a shift in steering from regime 1 to regime 3 in the evolution of the TC should be correlated with changes in the PV structure of the TC itself.

While this general structure of the PV tower does not change between regime 1 and regime 2-3, smaller-scale differences in the vertical distribution of PV may be able to help explain the change in steering sensitivity. The PV towers in both simulations at F42 (Figs. 2.10 g and h) are characterized by large regions of weak horizontal PV gradients. PV advection would therefore be localized to regions of maximum PV where horizontal PV gradients are strongest. The structure of the PV tower changes somewhat after the shift to regime 2 (Figs. 2.10 i and j). The minimum in horizontal PV gradient at these times is very close to the surface, and the horizontal PV gradient at low to mid levels has intensified throughout the core of the PV tower.

While there is still a clearly-defined PV maximum at mid to upper levels, contributions to PV advection from lower levels is clearly more important at times after the regime-shift than at times before. This may be an explanation for the regime-shift. During earlier times, the only strong PV gradients are concentrated at the location of the PV maxima themselves; in Helene-BM, this maximum occurs at mid to upper levels. As the cyclone matures, PV gradients intensify at lower levels, even though a consistent PV maximum is maintained at mid to upper levels (e.g., Fig 2.10i). The resulting advection is not simply the punctuated effect of advecting the PV maximum, but rather an integrated effect of advecting the entire PV tower. As a result, the optimal steering level moves down from the location of the PV maximum to a region which represents this column-integrated effect, the PV center of mass.

A similar analysis can be performed for the Grell simulation. At times before the regime-shift, again we see a single defined PV maximum, this time located at mid-to-lower levels. The PV tower builds vertically as the TC intensifies, and by the time the TC enters regime 2 (Fig. 2.10d) the PV maximum and PV center of mass have separated farther from one another in the vertical. The PV maximum is located at ~315 hPa, while the PV center of mass is down at ~500 hPa. The steering plot for this time shows a distinct minimum in the steering cost function for all steering columns centered on the PV center of mass. The PV structure of the TC at this time shows several distinct maxima. Between and outside these maxima, the horizontal gradient in PV weakens considerably, but is still stronger than it was in regime 1.

The PV structure of Helene-G at by regime 3 (Fig. 2.10k) differs from that observed in Helene-BM (Fig. 2.10l), but the effect is the same: the PV advection is no longer localized to a single region, and instead receives contributions from several levels rather than an amplification of the PV gradient throughout the depth of the PV tower as in Helene-BM. Despite the PV maxima at mid levels in the BM simulation, this tightening of the gradient provides significant contributions to PV advection from levels throughout the depth of the PV tower. The PV structure of the TC at later times for Helene-G is different, a sign of the differing cumulus parameterization changing the PV structure of the TC. In Fig. 2.10f, it is clear that the Grell parameterization does not tighten the PV gradient throughout the depth of the PV tower, but instead creates several localized PV maxima which are stacked on top of one another.

This structure, while different from the structure found in Helene-BM, appears to have a similar effect nonetheless. Rather than advection being localized to a single region, strong advection takes place at the location of each maximum, spreading out the effect of advection through a number of vertical levels. As a result, the significant region of advection moves from the singular PV maximum at early times to the PV center of mass at later times, the PV center of mass being an indication of a significant region of advection for the column-integrated advection of the entire PV tower.

e) Evidence of environmental shear in steering plots

As discussed previously, minima in steering cost function are not necessarily dependent solely on steering column depth. One may argue that whenever a minimum in steering cost function is strongly dependent on column depth, there must exist significant shear of the environmental wind. If the accuracy of a steering column centered at a particular level is dependent on the depth of that column, then significant environmental shear would cause strong variation in diagnosed steering between thin and deep columns. Likewise, it may be argued that whenever a minimum in steering cost function is independent of column depth, then the environmental shear must be weak.

However, the relationship is more complex. As a TC progresses through the three steering regimes, the location of the minimum in steering cost function moves from the PV maximum to the PV center of mass. The reason for this transition, as explained above, is that PV advection by the environmental flow changes from being localized at the level of the PV maximum (regime 1) to being contributed to by all levels throughout the depth of the PV tower (regimes 2 and 3). Once a TC reaches regime 3, the location of the minimum in steering cost function moves to the PV center of mass, because the PV center of mass behaves as the "steering level" for a TC when significant contributions to PV advection take place at many levels while the TC moves as a single entity.

With this in mind, one can return to Figure 2.12 and apply this understanding to the steering plots for Helene-G in regime 1 and regime 2 (Fig. 2.12b and 2.12d). In Fig. 2.12b, the steering cost function is minimized for columns centered on the PV maximum independent of column depth. Since a regime 1 TC is typified by PV advection localized to the level of the PV maximum, it is understood that the level of the PV maximum, unlike the level of the PV center of mass, does not correspond to some column-integrated PV advection. Therefore, in this scenario, there must be weak environmental shear in order for deep columns to be as accurate as shallow columns.

In Fig. 2.12d, a similar situation is presented. Steering cost function is minimized about a single layer, and again the minimum is independent of column depth. However, the TC is in regime 2, and the minimization occurs at the level of the PV center of mass. If a TC in a region of environmental shear moves as a single entity, we hypothesize that the steering level will be at the PV center of mass, corresponding to some column-integrated PV advection throughout the entire PV tower. As a result, we would expect steering cost function to be minimized at the PV center of mass in a regime 2 TC regardless of column depth. Deep columns provide a column-integrated steering flow, while thin columns at the PV center of mass provide the steering level of a regime 2 TC undergoing column-integrated PV advection. Figure 2.12d is essentially an example of proof-of-concept for PV center of mass steering.

The environmental wind in the vicinity of the TC is calculated by averaging the wind field within the horizontal domain of the steering column. This averaged flow, calculated on each level, can be thought of as the "environmental flow", because the symmetric flow of the TC vortex itself is removed. Figure 2.13 is a time-series plot of the magnitude of the standard deviation of this averaged flow between all 20 levels of the model for the Helene-BM and Helene-G simulations. Here, it is assumed that a high standard deviation of the averaged (environmental) wind indicates significant shear over the TC, while a low standard deviation implies that the shear over the TC is weak. While it is possible that

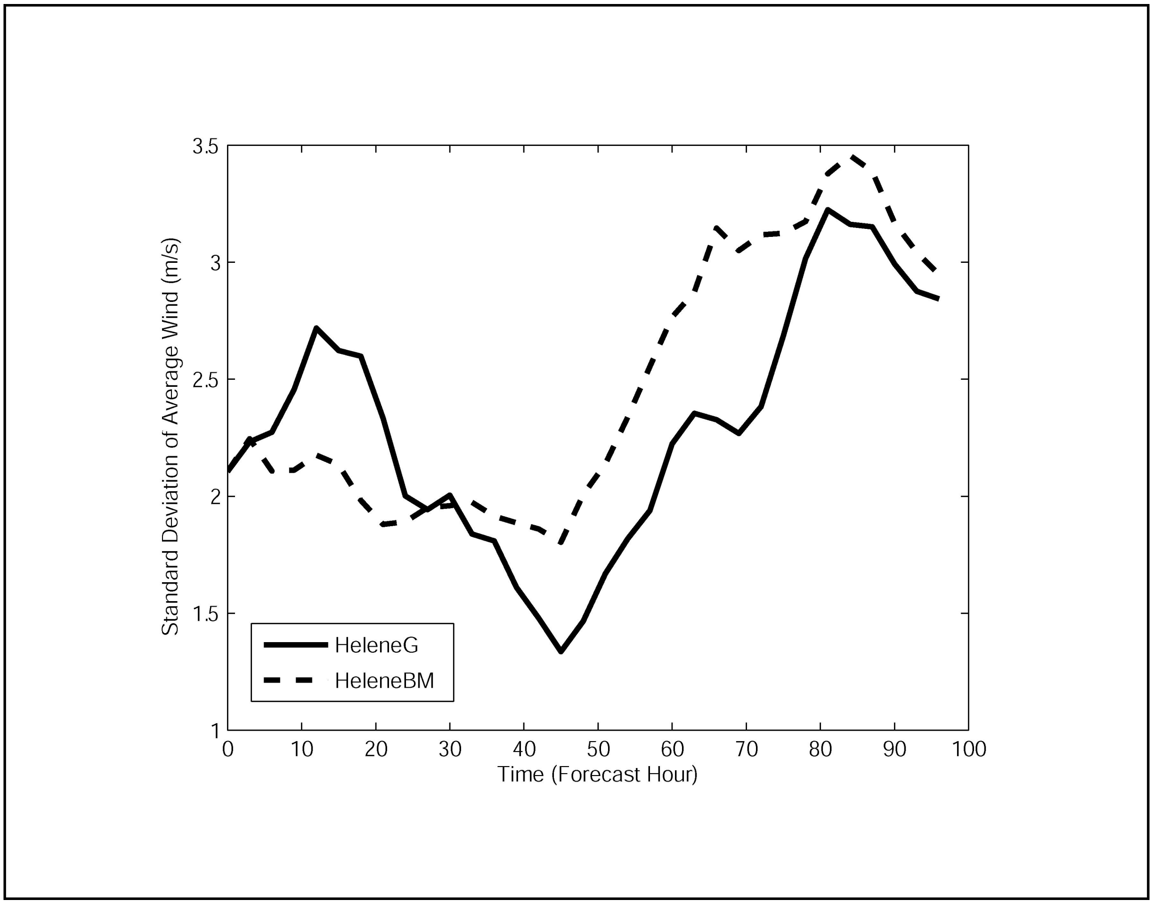

Figure 2.13. Time series of standard deviation of the environmental wind in Helene-BM and Helene-G simulations.

the differences in environmental wind with height may be organized such that no significant shear occurs over the TC itself, while strong differences arise at levels above the TC, we assume this to be rare, and that high standard deviation of the environmental wind indicates shear over the TC itself.

Focusing on the Helene-G curve, it's clear that Helene-G encounters strong standard deviation of environmental wind early on, and then reaches a minimum in standard deviation of less than 1.5 ms^{-1} at F42, when according to Figure 2.12b Helene-G is in regime 1 and the characteristics of the plot indicate that shear should be weak. Likewise, by F60 the standard deviation of environmental wind is over 2.0 ms^{-1} and rising steadily.

f) Minimization of the steering cost function around the vorticity center of mass and the vortex intensity - vortex depth relationship

By F84 (Figs. 2.12 e and f), both simulations have developed extremely similar steering cost function structures. In both simulations, steering cost function is minimized in a thin steering column centered about the PV center of mass. Indeed, it appears that the thinner the steering column becomes, the more accurate its diagnosis of TC motion. However, an equally accurate diagnosis of motion can be calculated when steering is estimated over a thick column centered on the vorticity center of mass. Like the previous minimum, this minimum in steering cost function is dependent upon column thickness, with steering cost function decreasing with increasing thickness. While this study is mainly concerned with the relationship between steering and TC PV structure, the consistent minimum in steering cost function about the vorticity center of mass cannot be ignored.

This minimum in steering cost function, related to the vorticity structure of the TC and dependent upon the depth of the steering column favoring deeper steering columns, may be a reflection of Velden and Leslie's vortex intensity – vortex depth (VI-VD) relationship. Because a TC's vortex tower builds vertically as the TC intensifies, one can imagine that the vorticity center of mass would likewise move upward as the TC intensifies. This migration of the vorticity center of mass upward would mean that more intense TCs have a vorticity center of mass closer to the middle (~500 hPa level) than less intense TCs, which would have a vorticity center of mass farther below. The closer the vorticity center of mass is to the middle of the model troposphere, the deeper a steering column centered on the vorticity center of mass can be calculated. Therefore, the most intense TCs would be typified by vorticity structures with the deepest steering columns to be centered about their vorticity center of mass. Since the deepest column centered on the vorticity center of mass minimizes the steering cost function, one can conclude that intense TCs are typified by deeper steering columns, while less intense TCs are typified by shallower steering columns. This is precisely the VI-VD relationship described in Velden and Leslie (1991). Interestingly, this relationship is observed only in the latest times of the simulation when the TC has reached peak intensity and maturity, and it appears to be completely disassociated with the minimum in steering cost function centered on the PV center of mass, which behaves quite differently.

g) *Analysis of track split*

1) SIMILARITIES OF LARGE-SCALE FLOWS

As discussed previously, the two simulations are nearly collocated for the first 12 to 15 hours, after which time a track split commences. Helene-G moves quickly to the northwest, while Helene-BM moves westward at a slower pace. After this initial track split, the two simulations continue to diverge, with Helene-BM taking a strong northward track while Helene-G continues to move to the northwest. By the end of both simulations, the two tracks have diverged by 475 km. The differential steering in these TC simulations at the time of the track split is important, because it marks a significant difference in the evolution of the steering in both simulations. After the track split, the two TCs are far enough apart that they are essentially being steered by two different environments. Even if they had the same PV structure, and therefore were typified by the same steering column structure, their tracks could continue to diverge because of differences in the environmental flow at their respective locations. Therefore, the time at which the track split occurs is the only time in which we can assume that the environmental flow at the location of each TC is the same (see below), and therefore any differences in TC motion at that time must be attributable to differences in steering column structure, or to non-steering processes which are not resolved using a PV advection approach to TC steering.

First we wish to rule out any significant differences in the environmental flow in the two simulations which could cause a change in steering even if the two simulations had identical steering column structure. Fig. 2.14 is a four-panel plot describing the steering of both simulations at F18. Fig. 2.14a is the steering plot for Helene-BM (same as Fig. 2.11). Figure 2.14b is a steering plot for Helene-G, assuming that Helene-G moves with the same speed and direction of Helene-BM. The two plots are similar, suggesting that the difference in environmental steering between the two simulations is small. In both Helene-BM and Helene-G, the same steering is diagnosed from a steering column centered about a region at low levels corresponding to the vorticity center of mass or very close to it. Relative maxima

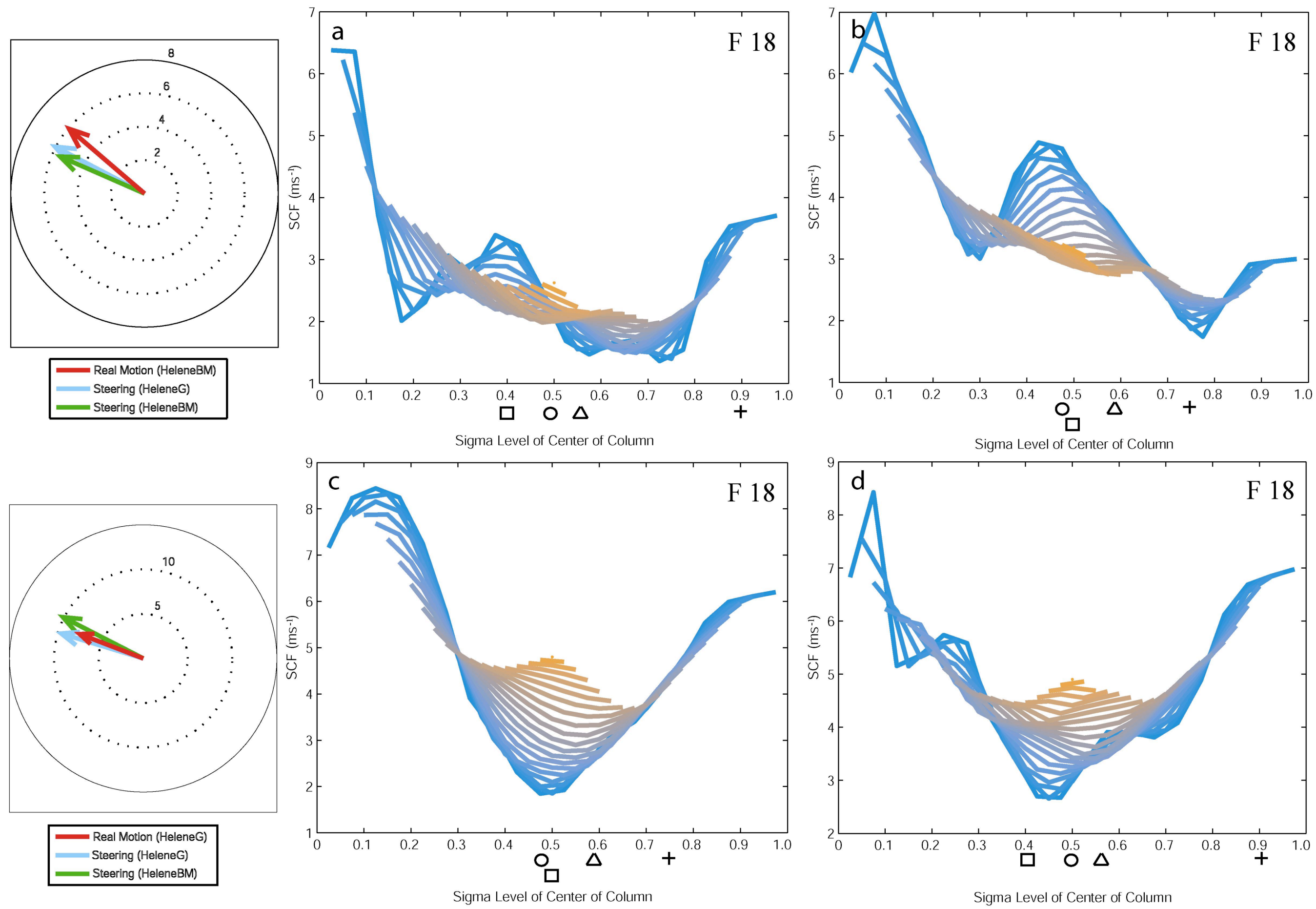

Figure 2.14. Steering plots testing the difference in environmental wind for both simulations at 18 hours into the simulation. Panel (a) is the steering plot for Helene-BM at F18. Panel (b) is an attempt to resolve the motion in the Helene-BM simulation using the Helene-G simulation to diagnose steering. Likewise, panel (c) is the steering plot for Helene-G at F18, while panel (d) is an attempt to resolve the motion in the Helene-G simulation using the Helene-BM simulation to diagnose steering. The similarity between panels (a) and (b), and between panels (c) and (d), suggest that the environmental flow is nearly identical in the region surrounding the TC in both simulations.

and minima in steering cost function at mid-to-upper levels are the same in both plots. To the left of these panels is a compass plot with vectors indicating the observed motion (MHMV) of Helene-BM, and the diagnosed steering from the optimal steering column using the environmental wind around Helene-BM and Helene-G.

Likewise, Fig. 2.14c is a steering plot for Helene-G at F18, while Fig. 2.14d is a steering plot resolving the motion of Helene-G in Helene-BM. The structure is very similar. A single minimum in steering cost function is found for thin steering columns centered at mid levels. This level corresponds to the PV maximum for Helene-G when Helene-G is used to diagnose the steering (Fig. 2.14c), and the level of minimum steering cost function shifts upward to the level of the PV maximum in Helene-BM when Helene-BM data is used (Fig. 2.14d). This demonstrates clearly that differences in environmental steering between the two simulations at this time are small. It can therefore be inferred that any differences in motions between the two simulations at this time are the result of non-steering processes.

The motion of Helene-G is consistent with "regime 1" behavior. Since we are analyzing steering at a time early in the life of the TC, we would expect that the PV structure of the cyclone is typified by strong PV advection localized to a single PV maximum. As a result, the level of the PV maximum is the optimal environmental level for diagnosing TC motion rests at the level of the PV maximum. Helene-BM, on the other hand, behaves quite differently. The optimal steering level is found in the region of the vorticity center of mass.

Another clear difference between the steering of Helene-BM and the steering of Helene-G at F18 is the significance of steering column depth. In Helene-G (Fig. 2.14c), the steering cost function is strongly dependent upon the depth of the steering column. As the depth of the steering column increases (as you progress from blue to orange lines on the steering plot), the steering cost function rapidly increases. By contrast, the minimum in steering cost function for Helene-BM at the same time (Fig. 2.14a) appears to be largely independent of the depth of the steering column. Since these are both regime 1 TCs at this time, this indicates a difference in the magnitude of wind shear over the two TCs (see part f). Indeed, a plot of standard deviation of environmental wind with height (Fig. 2.13) indicates that there is significantly higher standard deviation of environmental wind over Helene-G than Helene-BM. As a result, one would expect that Helene-G would produce a steering which is more sensitive to steering column depth than the more barotropic flow observed in Helene-BM.

While the difference in variance of environmental wind explains the differences in the steering with regard to column-thickness, it does not explain why Helene-G appears to be steered by PV advection while Helene-BM does not. The observed motion in Helene-BM does not appear to be explainable by the PV-steering approach. Here, we investigate non-steering processes which, combined with the PV-steering described in part d, describe the TC motion observed in Helene-BM, and what one can actually infer about the Helene-BM steering from the steering at F18 (Fig. 2.14a).

2) ROLE OF NON-STEERING PROCESSES

The PV tendency equation partitioned in this manner may be written as:

$$\frac{\partial q}{\partial t} = -\mathbf{V}_s \cdot \nabla q_s - \mathbf{V}_s \cdot \nabla q_{as} - \mathbf{V}_{as} \cdot \nabla q_s - \mathbf{V}_{as} \cdot \nabla q_{as} + \frac{Dq}{Dt},$$

where subscripts *s* and *as* denote respectively, the symmetric and asymmetric parts of the horizontal wind and PV. Chan et al. 2002 found that the steering process dominates for steady TC motion, while in erratic TC motion the two propagation mechanisms can play a large role. TC steering from this perspective can therefore be called "PV-steering". PV advection can be separated into two mechanisms. One mechanism is the advection of the symmetric component of PV by the environmental flow, which is the component of PV advection that describes TC steering from the PV perspective. It is referred to as asymmetric advection of symmetric PV, or AASPV, by Chan, Ko, and Lei (2002), where "asymmetric advection" refers to advection by the asymmetric, or environmental, component of the wind field in the vicinity of the TC. The other category, described by Chan, Ko, and Lei (2002), is the symmetric advection of asymmetric PV (SAAPV), where the asymmetric component of the PV in the TC is advected by the symmetric wind field about the cyclone itself. This component of PV advection is not resolvable through the PV-steering approach, because the symmetric component of the wind field about the TC necessarily vanishes when the horizontal averaging of the wind field is performed.

Chan (2005) explains that while the AASPV term is dominant for "steady" cyclone motion, when TC motion becomes erratic, it usually indicates that other terms in the PV tendency equation have more pronounced importance. Specifically, the contribution to PV tendency by diabatic heating, which when distributed asymmetrically through a TC can induce PV tendency in directions other than that caused by AASPV (Chan, Ko, and Lei 2002), and the SAAPV term. Often, the importance of diabatic heating and SAAPV are coincident, as asymmetric heating can produce asymmetric PV in the TC which is then advected around the TC by the symmetric wind field (Chan 2005).

Figure 2.15 is a six-panel plot of PV in the 650 hPa – 450 hPa layer for both simulations between F15 and F21. These are the times over which the MHMV is calculated for F18. At F15 (panels a and b) the PV in Helene-G is maximized at the location of the sea

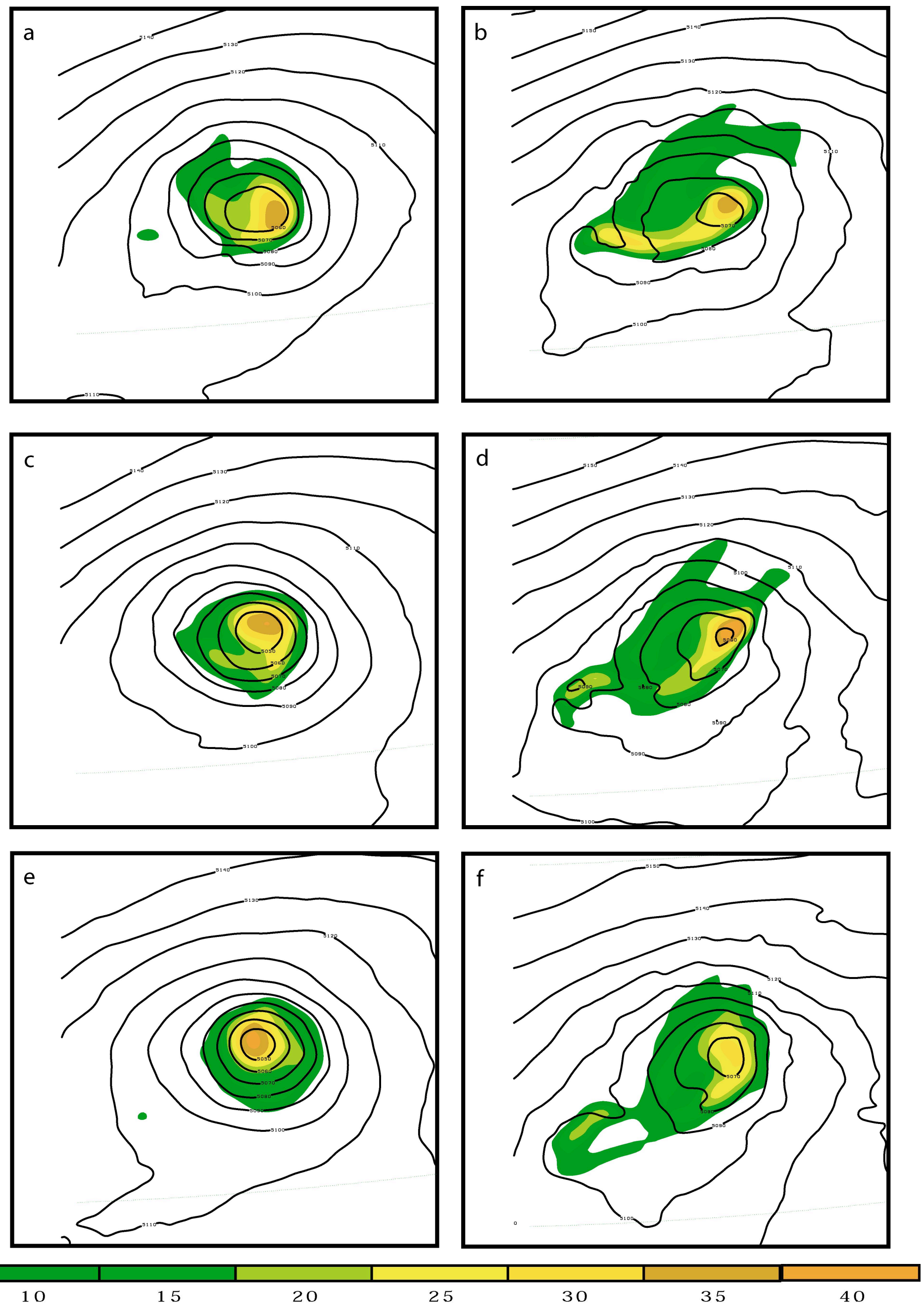

Figure 2.15. Six panel plot of potential vorticity (PV) in the 650 hPa – 450 hPa layer overlaid with geopotential heights at 550 hPa for 15 hours (panels a and b), 18 hours (panels c and d), and 21 hours (panels e and f) into the simulation. The left (right) panels correspond to the Helene-BM (Helene-G) simulation. PV is shaded every 0.5 PVU and heights are contoured every 10 m.

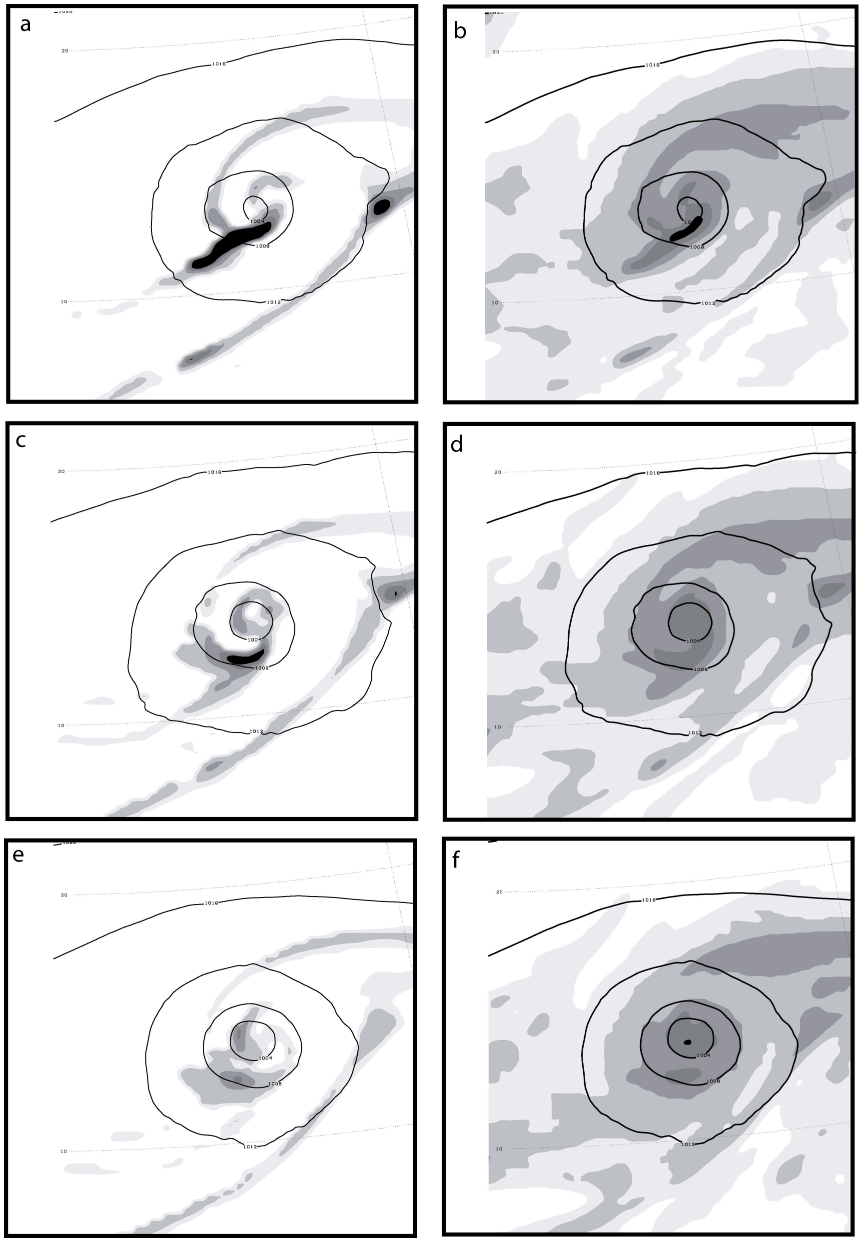

Figure 2.16. Plots of hourly precipitation (left) and surface saturated equivalent potential temperature (right) for Helene-BM at 15 hours (panels a and b), 18 hours (panels c and d), and 21 hours (panels e and f) into the simulation. Precipitation is plotted every 3 mmhr^{-1} between 3 mmhr^{-}1 and 12 mmhr^{-1}, and temperature is plotted every 3 K between 336 K and 348 K. Sea level pressure is overlaid, contoured every 4 hPa.

level pressure minimum, while in Helene-BM, the PV maximum appears in the southeast corner of the TC. Over the next six hours (panels c and e) large amounts of asymmetric PV are advected northward within the center of the vortex, as well as eastward along the periphery of the vortex center. As a result, Helene-BM experiences significant SAAPV as the PV maximum is advected cyclonically around the center of the TC. This propagation mechanism contributes a component to the PV tendency which does not appear in Helene-G.

While no direct analysis of diabatic heating is performed, plots of precipitation show that strong asymmetric precipitation takes place in the southeast quadrant of Helene-BM over the same time period, coincident with the surface saturated equivalent potential temperature maximum (Fig. 2.16). The asymmetric diabatic heating, together with the SAAPV, contribute a northeastward component to PV tendency in Helene-BM, and an analysis of three-layer deep steering columns at F18 (Fig. 2.17) indicates that this component, together with AASPV from steering at the level of the PV maximum, closely predicts TC motion in Helene-BM.

This analysis indicates that the track-split observed between Helene-BM and Helene-G is not explainable through the PV-steering perspective, because TC steering only encompasses the asymmetric advection of the symmetric component of PV in the TC. When Helene-BM begins to change direction, the diabatic heating and SAAPV terms become dominant. The slowing of TC motion in Helene-BM is therefore due to a ‘wobble’ in the asymmetric PV of the TC as it’s advected eastward and northward into the cyclone center, together with PV tendency from asymmetric diabatic heating. Helene-G maintains a more steady track and TC motion is largely described by the AASPV term, resolvable by the PV-steering perspective. This is consistent with the analysis of these terms in PV tendency by

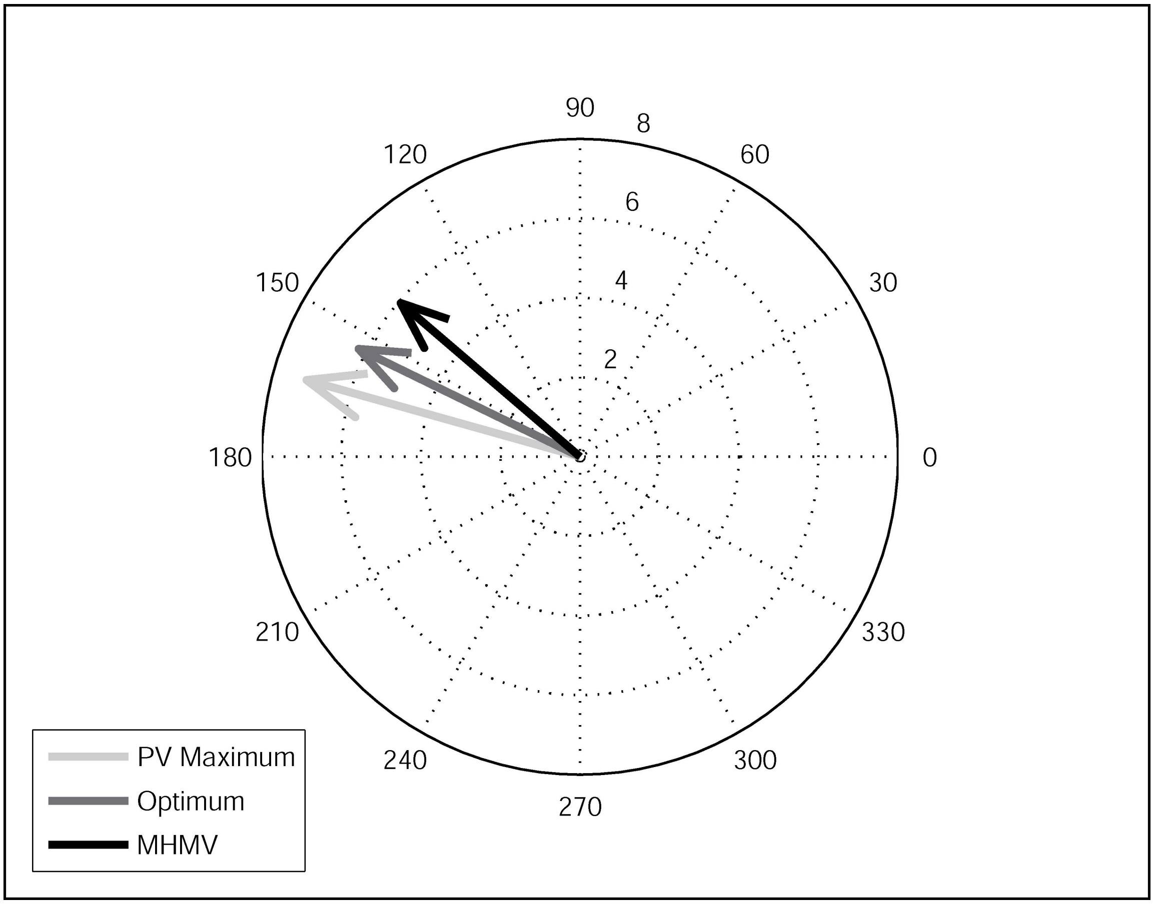

Figure 2.17. Vectors describing the MHMV for Helene-BM at 18 hours into the simulation, the 3-sigma-layer deep diagnosed steering centered on the PV maximum, and the optimum 3-sigma-layer deep diagnosed steering.

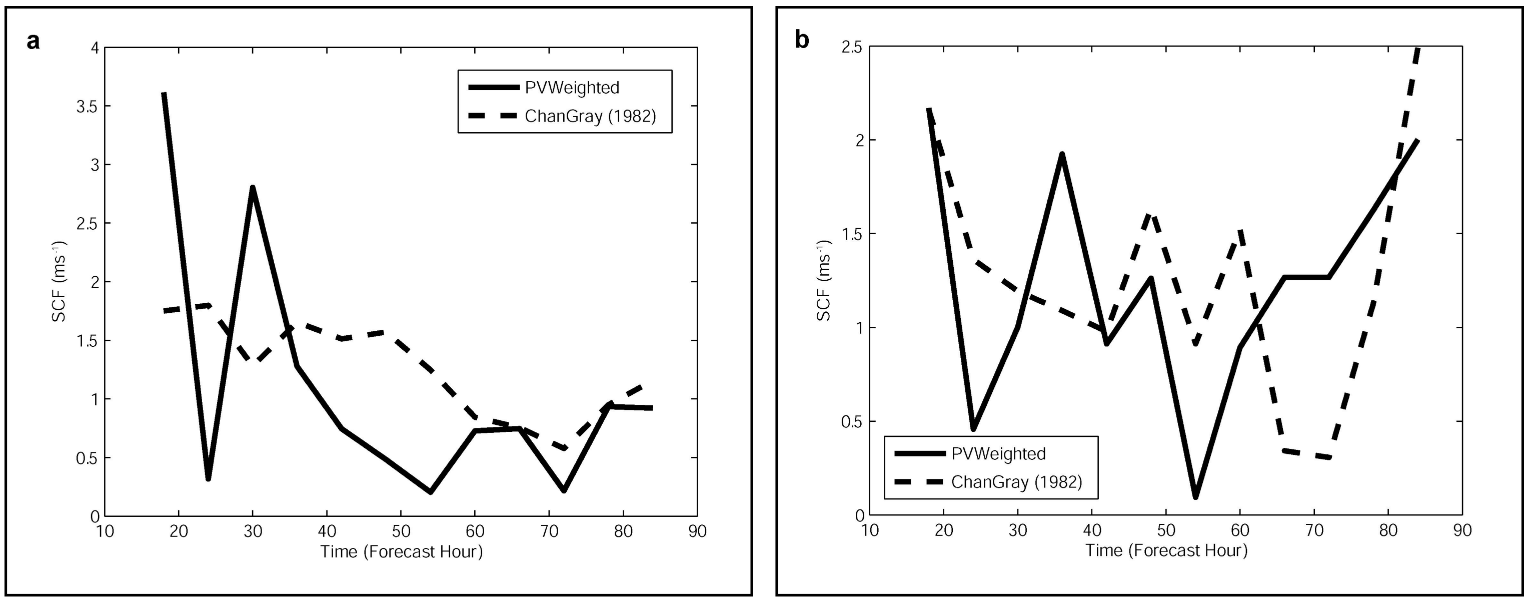

Figure 2.18. Steering cost function (SCF) in PV-weighted steering flow for each analyzed time, as compared to the error of a steering column as defined by Chan and Gray (1982). Panel (a) is for Helene-G, and panel (b) is for Helene-BM.

Chan (2005).

h) A PV-weighted steering flow perspective

As a final experiment, the PV in the vicinity of the TC was used to directly weight the winds in the averaging box at each time to derive a “PV-weighted steering flow”. This method has the benefit of being largely independent of the size of the averaging box.

Figure 2.18 is a plot of the steering cost function in the PV-weighted steering over time for each simulation, compared to the steering cost function in steering for a steering column as defined by Chan and Gray (1982). The overall trend in the steering cost function for Helene-G (Fig. 2.18a) is downward, with high (3.5 ms^{-1}) steering cost function at F18, and quickly dropping to within 1.0-1.5 ms^{-1} steering cost function by F36. The PV weighted steering flow appears to outperform the Chan and Gray (1982) steering column throughout the simulation beyond the first 36 hours. For Helene-BM (Fig. 2.18b) the PV weighted steering flow maintains a steering cost function of less than 2 ms^{-1} throughout the simulation, but there is no obvious downward trend, nor does it consistently outperform the steering column as defined by Chan and Gray (1982).

Results of the PV weighted steering flow are mixed. The steering cost function for the PV-weighted steering flow and the Chan and Gray (1982) steering column for Helene-BM at F18 are nearly identical, owing to the fact that there is significant contribution to PV tendency by propagation mechanisms which are not resolved by steering, no matter how it is defined. Similar propagation events coincide with peaks in steering cost function at F30 for Helene-G and F36 for Helene-BM. The peak in steering cost function for Helene-G at F18 is likely due to the strong dependence of steering on column depth at that time; optimum steering is confined to a thin layer at the level of the PV maximum while the PV distribution is not.

2.5 Summary and conclusions

It has been shown that significant variations in the track of a modeled TC arise from the way an NWP model allows sub-grid scale (i.e., parameterized) convection to influence grid-scale model variables through the CPS. For the case considered, a simulation of Helene (2006) it has been shown that the observed track split due to differences in the chosen cumulus parameterization scheme is attributable to differences in the cyclone-scale PV advection and non-conservation rather than differences in the manner in which the large-scale environment advects the TC.

The initial track split has been shown to be caused by the distribution of asymmetric PV in the core of the modeled TC, and how that PV influences or is influenced by the symmetric flow about the TC. In Helene-BM, asymmetric PV is created and undergoes significant advection by the symmetric wind field between 15 and 21 hours into the simulation, causing a propagation of the TC to the northeast, whereas Helene-G produces asymmetric PV which instead appears to adjust the wind field of the TC rather than be advected by it. As a result, the motion of Helene-G closely follows advection by the asymmetric flow, while the motion of Helene-BM deviates from this advection.

The PV tendency equation was applied to the steering of the modeled TC when advection of the TC PV by the asymmetric wind became the dominant mechanism. The definition of the steering flow depends on the characteristics of the steering column over which the horizontal winds are averaged to obtain the asymmetric flow. Through the use of the steering plot, the characteristics of the optimal steering column can be related to the PV and vorticity structure of the TC itself.

The steering plot reveals three steering regimes through which the modeled TC progresses. Furthermore, these regimes can be directly related to the PV structure of the TC. In regime 1, the PV structure of the TC is typified as a single PV maximum embedded in a weak horizontal PV gradient throughout the PV tower. As a result, significant contributions to the advection of the PV tower by the asymmetric flow are confined to the level of the PV maximum. As the TC matures, it enters regime 2, when significant contributions to PV advection by the asymmetric wind come from levels throughout the PV tower. As a result, the optimal steering column is no longer found at the level of the PV maximum, but instead at the level of the PV center of mass. Finally, in regime 3, a clear structure emerges where the optimal steering column can either be a thin column centered on the PV center of mass, or a deep column centered on the vorticity center of mass. The deep column centered on the vorticity center of mass can be related to the VI-VD relationship by Velden and Leslie (1991).

Clearly, while the separation between "TC flow" and "environmental flow" is non-unique, it is not without constraints. By treating the TC as a cyclonic PV tower, and the steering of the TC as the advection of the PV tower by the asymmetric flow, the characteristics of the optimal steering column can be related to the PV structure of the TC. Like the VI-VD relationship, the characteristics of the optimal steering column appear to be related to the intensity of the TC, but from a PV perspective, the relationship becomes more complicated. More so than the intensity of the PV tower, the organization of the PV within the tower appears to have a significant impact on TC steering. It is widely known that models are able to forecast TC track with far greater accuracy than they can forecast TC intensity (DeMaria and Gross 2003). This is further evidence that the storm-scale PV structure is the characteristic which dictates the optimal steering column, rather than intensity. While CPSs use a variety of tactics and constraints to produce realistic convection and accurately adjust model variables to the presence of that convection, for TC steering it appears that forecasting accuracy may be a function of how realistically the PV is redistributed within the core of the TC due to the convection. Further research is required to adequately analyze the effect of various CPSs on the PV structure of the modeled TC, how realistic that structure is compared to actual observations, and ultimately how that accuracy is reflected in TC track forecasting accuracy.

Chapter 3

3.1 Future work and conclusions

It has been shown that the steering of a modeled TC can be significantly changed by changing the CPS within the model. Here, TC steering has been described as the advection of the TC PV structure by an asymmetric, “environmental flow”. The environmental flow is defined as the full, modeled horizontal flow minus the vertically and horizontally averaged (symmetric) component of the horizontal flow centered on the position of the TC. Since the definition of the environmental flow depends on the dimensions of the steering column over which the horizontal winds are averaged, it is non-unique. However, the characteristics of the optimal steering column can be related to the PV and vorticity structure of the TC.

While differences in large-scale environment appear over time between two simulations varying only in choice of CPS, it has been shown that these differences are too small to sufficiently explain why the TC track diverges between the two model simulations after less than 24 hours. While the track split was not due to differences in steering between the simulations, the propagation mechanisms which cause the initial split are fully explained by the PV tendency. Furthermore, while storm-scale differences in generation and behavior of asymmetric PV lead to propagation of the TC, evidence has been presented to suggest that similar scale changes to PV distribution within the core of the TC have a significant effect on the characteristics of the optimal steering column.

The steering plot has been introduced as a useful diagnostic tool for comparing the characteristics of the optimal steering column to the PV and vorticity structure of the TC. Through these plots, it has been shown that the relationship of optimal steering column structure to TC structure (specifically TC PV structure) is more complicated than the VI-VD relationship described in Velden and Leslie (1991). For the case considered, the relationship of steering column structure to TC PV structure appears to be separated into three regimes in the early development of the TC. These regimes are due to the development of the symmetric TC PV as the TC matures. In regime 1, the optimal steering column is found centered at the level of the maximum PV in the TC, because the PV structure of the TC at the earliest stages confines significant PV advection to this level. In regime 2, the PV structure of the TC matures, and significant contributions to PV advection takes place at many levels of the troposphere. In such a case, we can define a PV "center of mass", describing the new level at which a steering column is optimized. In regime 3, the TC's PV structure is fully mature, and the steering plot takes on a clear structure, with a thin optimal steering column centered on the PV center of mass, and an equally optimal deep steering column centered on the vorticity center of mass. This deep optimal steering column may be thought of as a confirmation of the VI-VD relationship described by Velden and Leslie (1991) for more intense TCs.

As evidenced by DeMaria and Gross (2003), NWP models can forecast TC track with significantly greater accuracy than they can forecast TC intensity, and TC track forecasting accuracy has improved over time at a much faster rate. This fact alone makes it clear that the characteristics of the optimal steering column cannot be a function of the intensity of the modeled TC alone. The evidence from this study makes it clear that TC steering is a function of PV distribution at the storm scale, and while two simulated TCs can be in nearly identical environments and be nearly the same intensity, a track split can still occur.

With regard to accuracy of TC track forecasting, the underlying question of why one CPS may produce a far more accurate TC forecast position while another does not, even in the face of poor intensity forecasting, is still unanswered. Furthermore, the lack of in-situ observations in the region of the TC core presents a challenge to NWP model development in this area. If, as evidenced by this study, the steering of the TC is dictated by the distribution of PV within the core of the TC, then it is clear that greater TC track forecasting accuracy can be gained by using a CPS which redistributes PV within the core of the TC in a realistic way.

First, observational and analysis campaigns are required to provide information on the real distribution of PV within the core of the TC and how that distribution changes as the TC matures. In this study, it was found that the two CPSs provided significantly different PV distributions at storm scale. The BM CPS developed a PV tower with a single maximum in the mid-troposphere and a strong horizontal PV gradient throughout the depth of the PV tower as the TC matured. The Grell CPS, on the other hand, developed isolated PV maxima within the PV tower, stacked vertically on one another. While track forecast accuracy was not a goal of this study, it is clear that the Grell CPS produced a more accurate TC track, even though the intensity forecast was significantly worse than the simulation using the BM CPS. A more realistic PV distribution within the core of the PV tower, if such is the case, could be one factor contributing to a more realistic TC track. Without observation data of this sort, such a comparison cannot be made.

Secondly, the specific effect of the CPS on the TC PV structure needs to be investigated. CPSs use a variety of constraints and tactics for determining where convection takes place, and how model variables are changed by sub-grid scale convection. In this experiment, the BM CPS adjusts thermal and moisture profiles with the goal of maintaining realistic profiles of these variables during deep convection. By contrast, the Grell parameterization uses a quasi-equilibrium scheme and is largely concerned with the removal of conditional instability from the large scale flow through consuming moist static energy. These are two wildly different philosophies on how cumulus convection affects the model variables, and it comes as no surprise that they produce significantly different PV structures within the core of the TC. However, the specific reason why a particular CPS produces a particular PV profile has not been explored. While the BM CPS has a stated goal of attempting to maintain realism, it is not certain that the PV redistribution caused by the cumulus convection is realistic.

Finally, it must be mentioned that any study of TCs using a CPS is inherently unrealistic. While the CPS is able to adjust the PV distribution of the TC through dictating the diabatic heating profile, the CPS is essentially unable to account for vertical momentum transport within the TC. Even a CPS which accounts for the effects of convective downdrafts, like the Grell scheme used here, will only adjust the thermal field to simulate the downdrafts. As a result, one can think of the CPS as only being able to account for 50% of the PV redistribution within the TC; it can adjust the thermal field but not the wind field. This is an essential limitation of the CPS, which can only be overcome if the model is run at high enough resolution to forego the use of any CPS and instead resolve convection explicitly. While these results do not specifically pertain to such a simulation, the basic idea of TC steering as a PV advection process could still easily be tested within this more realistic framework. Such a simulation would need to be performed to create a useful application for these results, and the lower resolution CPS simulations could be compared to the high resolution simulation to see if there is any correlation between TC track prediction and realistic TC PV distribution.

References

Arakawa, A., and W.H. Schubert, 1974: Interaction of a cumulus cloud ensemble with the large-scale environment, Part I. *J. Atmos. Sci.*, **31**, 674–701.

Baik, J.J., M. DeMaria, and S. Raman, 1990: Tropical cyclone simulations with the Betts convective adjustment scheme. Part I: Model description and control simulation. *Mon. Wea. Rev.*, **118**, 513–528.

Betts, A. K., 1986: A new convective adjustment scheme. Part I: Observational and theoretical basis. *Quart. J. Roy. Meteor. Soc.*, **112**, 1306-1335.

_____, and M. J. Miller, 1986: A new convective adjustment scheme. Part II, Single column tests using GATE wave, BOMEX, and arctic air-mass data sets. *Quart. J. Roy. Meteor. Soc.*, **112**, 693-709.

_____, and _____, 1993: The Betts-Miller scheme. *The Representation of Cumulus Convection in Numerical Models of the Atmosphere, Meteor. Monogr.*, No. 46, Amer. Meteor. Soc., 107-121.

Chan, J.C.L., F.M.F. Ko, and Y.M. Lei, 2002: Relationship between potential vorticity tendency and tropical cyclone motion. *J. Atmos. Sci.*, **59**, 1317–1336.

_____, and W.M. Gray, 1982: Tropical cyclone movement and surrounding flow relationships. *Mon. Wea. Rev.*, **110**, 1354–1374.

_____, 2005: The physics of tropical cyclone motion. *Annu. Rev. Fluid Mech.*, **37**, 99-128.

DeMaria M., and J. M. Gross, 2003: Evolution of tropical cyclone forecast models. *Hurricane! Coping with Disaster*, R. Simpson, Ed., Amer. Geophys. Union, 103–126.

Dong, K., and C.J. Neumann, 1986: The relationship between tropical cyclone motion and environmental geostrophic flows. *Mon. Wea. Rev.*, **114**, 115–122.

Emanuel, K. A. 1994. *Atmospheric convection. Oxford University Press. New York.*

Emanuel, K. A., 2007. Personal Correspondence.

Fiorino, M., and R.L. Elsberry, 1989: Some aspects of vortex structure related to tropical cyclone motion. *J. Atmos. Sci.*, **46**, 975–990.

Flatau, M., W.H. Schubert, and D.E. Stevens, 1994: The role of baroclinic processes in tropical cyclone motion: the influence of vertical tilt. *J. Atmos. Sci.*, **51**, 2589–2601.

Grell, G.A., 1993: Prognostic evaluation of assumptions used by cumulus parameterizations.

Mon. Wea. Rev., **121**, 764–787.

_____, J. Dudhia, and D. R. Stauffer, 1995: A description of the fifth generation Penn State/NCAR mesoscale model (MM5). NCAR Tech Note NCAR/TN-3981STR, 138 pp. [Available from NCAR Publications Office, P. O. Box 3000, Boulder, CO 80307-3000.]

Haagenson, Phillip L. et al. 1994. *The Penn State/NCAR Mesoscale Model (MM5): Source Code Documentation. NCAR/TN-392 + STR.* National Center for Atmospheric Research. Boulder, Colorado.

Pike, A.C., and C.J. Neumann, 1987: The variation of track forecast difficulty among tropical cyclone basins. *Wea. Forecasting*, **2**, 237–241.

Prater, B. E., and J. L. Evans, 2002: Sensitivity of modeled tropical cyclone track and structure of Hurricane Irene (1999) to the convective parameterization scheme. *Meteor. Atmos. Phys.,* **80,** 103–115.

Shapiro, L.J., 1992: Hurricane vortex motion and evolution in a three-layer model. *J. Atmos. Sci.*, **49**, 140–154.

_____, 1996: The motion of Hurricane Gloria: a potential vorticity diagnosis. *Mon. Wea. Rev.*, **124**, 2497–2508.

_____, and J.L. Franklin, 1995: Potential vorticity in Hurricane Gloria. *Mon. Wea. Rev.*, **123**, 1465–1475.

Simpson, R. H., 1971: The decision process in hurricane forecasting. NOAA Tech. Memo. NWS SR-53, 35 pp.

Smith, R. K., 2000: The role of cumulus convection in hurricanes and its representation in hurricane models. *Rev. Geophys.,* **38,** 465–489.

Ueno, M., 2003: Steering weight concept and its application to tropical cyclones simulated in a vertical shear experiment. *J. Meteor. Soc. Japan*, **81**, 1137-1161.

Velden, C.S., and L.M. Leslie, 1991: The basic relationship between tropical cyclone intensity and the depth of the environmental steering layer in the Australian region. *Wea. Forecasting*, **6**, 244–253.

Wada, M. 1979. Numerical experiments of the tropical cyclone model by use of the Arakawa-Schubert parameterization. *J. Meteor. Soc. Japan*, **57**, 505-530.

Wang, W., and N.L. Seaman, 1997: A comparison study of convective parameterization schemes in a mesoscale model. *Mon. Wea. Rev.*, **125**, 252–278.

Wu, C.C., and K.A. Emanuel, 1993: Interaction of a baroclinic vortex with background shear: application to hurricane movement. *J. Atmos. Sci.*, **50**, 62–76.

_____, and _____, 1995: Potential vorticity diagnostics of hurricane movement. Part 1: A case study of Hurricane Bob (1991). *Mon. Wea. Rev.*, **123**, 69–92.

_____, and _____, 1995: Potential vorticity diagnostics of hurricane movement. Part II: Tropical Storm Ana (1991) and Hurricane Andrew (1992). *Mon. Wea. Rev.*, **123**, 93–109.

_____, and Y. Kurihara, 1996: A numerical study of the feedback mechanisms of hurricane–environment interaction on hurricane movement from the potential vorticity perspective. *J. Atmos. Sci.*, **53**, 2264–2282.

Wu, L., and B. Wang, 2000: A potential vorticity tendency diagnostic approach for tropical cyclone motion. *Mon. Wea. Rev.*, **128**, 1899–1911.

_____, and _____, 2001: Effects of convective heating on movement and vertical coupling of tropical cyclones: a numerical study. *J. Atmos. Sci.*, **58**, 3639–3649.

Support

I would like to make special mention of three organizations which have supported me in this research. This research was funded by a National Science Foundation Grant ATM-0125169, and from the Office of Naval Research, project number 144PN07. I also received the American Meteorological Society 21st Century Campaign Graduate Fellowship.